Christie, D.M., Pedersen, R.B., Miller, D.J., et al., 2001
Proceedings of the Ocean Drilling Program, Initial Reports Volume 187

2. EXPLANATORY NOTES[1]

Shipboard Scientific Party[2]

INTRODUCTION

This chapter contains information that will help the reader understand the basis for our preliminary conclusions and help the interested investigator select samples for further analysis. This information concerns only shipboard operations and analyses described in the site reports in the *Initial Reports* volume of the Leg 187 *Proceedings of the Ocean Drilling Program*. Methods used by various investigators for shore-based analyses of Leg 187 data will be described in the individual scientific contributions published in the *Scientific Results* volume and in various professional journals.

Authorship of Site Chapters

The separate sections of the site chapters were written by the following shipboard scientists, listed in alphabetical order:

Leg Summary: David Christie, Rolf B. Pedersen
Operations: Ron Grout, Jay Miller
Igneous Petrology and Geochemistry: Vaughn Balzer, David Christie, Florence Einaudi, Margaret Gee, Folkmar Hauff, Pamela Kempton, Christine Meyzen, Rolf B. Pedersen, Douglas Pyle, Christopher Russo
Alteration: Folkmar Hauff, Jay Miller, Ingunn Thorseth
Microbiology: Kristine Lysnes, Ingunn Thorseth
Structural Geology: Hiroshi Sato
Underway Geophysics: Wen-Tzong Liang
Core Descriptions: Shipboard Scientific Party

[1]Examples of how to reference the whole or part of this volume.
[2]Shipboard Scientific Party addresses.

Ms 187IR-102

Numbering of Sites, Holes, Cores, and Samples

Drilling sites are numbered consecutively from the first site drilled by the *Glomar Challenger* in 1968. A site refers to one or more holes drilled while the ship was positioned over a single acoustic beacon. Multiple holes are often drilled at a single site by pulling the drill pipe above the seafloor (out of the hole), offsetting the ship some distance from the previous hole (without deploying a new acoustic beacon), and drilling another hole.

For all Ocean Drilling Program (ODP) drill sites, a letter suffix distinguishes each hole drilled at a single site. The first hole at a given site is assigned the suffix A, the second hole is designated with the same site number and the suffix B, and so on. Note that this procedure differs slightly from that used by the Deep Sea Drilling Project (DSDP) for Sites 1 through 624 but prevents ambiguity between site- and hole-number designations. These suffixes are assigned regardless of recovery, as long as penetration takes place. Distinguishing among holes drilled at a site is important because recovered rocks from different holes, particularly when recovery is <100%, often represent different intervals in the cored section.

The cored interval is measured in meters below seafloor (mbsf); subbottom depths assigned to individual cores are determined by subtracting the drill-pipe measurement (DPM) water depth (the length of the pipe from the rig floor to the seafloor) from the total DPM (from the rig floor to the bottom of the hole; see Fig. **F1**). Water depths below sea level are determined by subtracting the height of the rig floor above sea level from the DPM water depth. The depth interval assigned to an individual core begins with the depth below the seafloor at which the coring operation began and extends to the depth that the coring operation ended for that core (see Fig. **F1**). Each coring interval is equal to the length of the joint of drill pipe added for that interval (~9.4–10.0 m). The pipe is measured as it is added to the drill string, and the cored interval is usually recorded as the length of the pipe joint to the nearest 0.1 m. However, coring intervals may be shorter and may not be adjacent if these are separated by intervals drilled but not cored or by washed intervals.

Cores taken from a hole are numbered serially from the top of the hole downward. Core numbers and their associated cored intervals (in mbsf) are usually unique in a given hole; however, this may not be true if an interval must be cored twice because of caving of cuttings or other hole problems. The maximum full recovery for a single core is 9.5 m of rock contained in a core barrel (6.6-cm internal diameter). Only rotary coring bits were used on Leg 187.

Leg 187 targeted exclusively hard-rock cores, which were curated following ODP protocols. According to these protocols, cores are pulled from the core barrels in butylate liners, split into ~1.5-m sections, and transferred into split, 1.5-m butylate core liners for curation and storage. The bottoms of oriented pieces (i.e., pieces that could not have rotated about a horizontal axis in the core barrel) are marked with a red wax pencil to preserve orientation during the splitting and labeling process. Contiguous pieces with obvious features allowing realignment are considered to be a single piece. Plastic spacers are used to separate the pieces. The cores are then split into archive and working halves. In splitting the core, every effort is made to ensure that important features are represented in both halves. Each piece is numbered sequentially from the top of every section, beginning with number 1; reconstructed

F1. Coring operations and core recovery terms, p. 23.

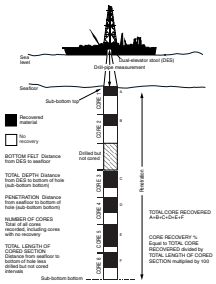

groups of pieces are lettered consecutively (e.g., 1A, 1B, 1C, etc.; see Fig. F2). Pieces are labeled only on external surfaces, and, if oriented, a way-up arrow is added to the label. Visual core descriptions are prepared for the archive half, which is then photographed with both black-and-white and color film, one core at a time. Nondestructive paleomagnetic measurements are performed on the archive halves of cores, unless the cores were broken into pieces too fine to make the measurements meaningful. The working half is sampled for shipboard and shore-based studies. Records of all samples are kept by the curator at ODP. Both halves of the core then are shrink-wrapped in plastic to prevent rock pieces from vibrating out of sequence during transit, placed into labeled plastic tubes, sealed, and transferred to cold-storage space aboard the drilling vessel. All Leg 187 cores are stored at ODP's Gulf Coast Repository at Texas A&M University in College Station.

When the recovered core is shorter than the cored interval, the top of the core is equated with the top of the cored interval by convention to achieve consistency when handling analytical data derived from the cores. Samples removed from the cores are designated by distance measured in centimeters from the top of the section to the top and bottom of each sample removed from that section. A complete identification number for a sample consists of the following information: leg, site, hole, core number, core type, section number, piece number (for hard rock), and interval in centimeters measured from the top of the section. For example, a sample identification of "187-1152A-10R-1, 10–12 cm" represents a sample removed from the interval between 10 and 12 cm below the top of Section 1, Core 10 (R designates that this core was taken with a rotary coring bit) of Hole 1152A, cored during Leg 187.

Recovery rates are calculated based on the total length of a core recovered divided by the length of the cored interval (see Fig. F1). As hard-rock coring operations are characterized by <100% recovery, the spacers between pieces can represent intervals of no recovery up to the difference in length between a cored interval and the total core recovered. Total core recovery is calculated by shunting the rock pieces together and measuring to the nearest centimeter; this information is logged into the shipboard database. Most cores are designated R for curatorial purposes. In instances where coring intervals exceed the 9.5-m length of the core barrel, cores are curated as wash intervals and labeled W. Photographs of each core and detailed descriptions of each core sampled and of thin-sections are provided (see the "Core Descriptions" contents list).

Sediment cores commonly include material recovered in the core catcher. Unlike hard-rock recovery, this material is not included in the lowermost section of core but is curated as Section CC. During Leg 187, rare intervals were recovered without new penetration because of hole collapse or other fill. An artifact of the curation database requires these cores to be archived as G (ghost cores).

F2. Core curation procedures for hard rocks, p. 24.

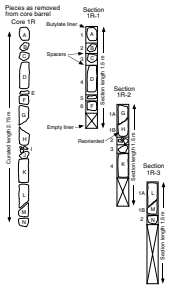

Summary Core Descriptions

To aid the interested investigator, we have compiled summary information of core descriptions on a section-by-section basis and presented these on hard-rock visual core description (HRVCD) forms (see the "Core Descriptions" contents list). These forms (Fig. F3) summarize the igneous, alteration, metamorphic, and structural character of the core; they also present graphical representations of the pieces recovered and the lithologic units defined. In the CD-ROM and World Wide Web

F3. Example of a basalt HRVCD form, p. 25.

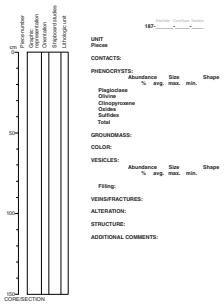

publication formats, these forms contain a link to an image of the archive half of the core captured shortly after splitting. On the left-hand side of the form, several columns record information about the core. In right-to-left sequence, these columns include (1) archived piece numbers; (2) sketches of each piece with details (veins, fractures, etc.) added to help distinguish features in the image; (3) arrows indicating way up for oriented pieces; (4) the next locations of shipboard samples marked according to the sampling code in the Janus database (XRF = X-ray fluorescence analysis; TSB = polished thin-section billet; XRD = X-ray diffraction analysis; ICP = inductively coupled plasma spectrometry analysis; BIO = microbiological sample); and (5) a unit number for each lithologic unit. On the right-hand side of these forms is a text summary of observations from every section, including (1) upper and lower contacts of each lithologic interval; (2) primary lithology; (3) comments summarized from rock descriptions; and (4) structural information.

IGNEOUS PETROLOGY

The procedures and methods for igneous rock core descriptions used during Leg 187 generally follow those adopted during Leg 183 (Coffin, Frey, Wallace, et al., 2000), and much of the discussion presented here comes from that source. Observations on hard-rock petrology and petrography were stored in ODP written and electronic media according to the definitions given below. Macroscopic observations on igneous rocks were recorded on HRVCD forms by the igneous petrologists.

Visual Core Descriptions

HRVCD forms were used to document each section of the igneous rock cores. The left column on the form, adjacent to the core photograph, graphically represents the archive half. A horizontal line across the width of this column denotes a plastic spacer. Oriented pieces are indicated on the form by an upward-pointing arrow to the right of the piece. Locations of samples selected for shipboard studies are indicated in the column headed "Shipboard Studies" with notation as described in **"Introduction,"** p. 12, in "Geochemistry."

Written descriptions accompanying the schematic representation of the core sections include the following information for each unit:

1. The lithologic unit number (numbered consecutively downhole, see **"Designation of Lithologic Units,"** p. 5, for details), rock name (see **"Rock Classification,"** p. 5, for details), and the piece numbers.
2. Descriptions of contact relationships with neighboring lithological units and of contact relationships within lithologic units. The latter may include descriptions of textural variations across chilled margins and note the presence of sediment adhering to pillow lava pieces or occurring between clasts in rubble or talus.
3. A list of phenocryst types visible with a hand lens or a binocular microscope, their distribution, abundance, size, shape, degree of alteration, and other characteristics.
4. A description of groundmass texture and grain size, following the definitions provided in Williams et al. (1982), such as glassy, microcrystalline (i.e., requires a petrographic microscope to distinguish individual crystals), fine grained (<1 mm but large

enough to identify with a hand lens), medium grained (1–5 mm), or coarse grained (>5 mm); variations in grain size within units were also noted.
5. The abundance of vesicles by volume, their distribution, size, shape, and the presence of mineral linings and fillings.
6. A description of color.
7. A description of the rock structure (i.e., whether the unit is massive, flow-banded, flow-brecciated, scoriaceous, pillowed, hyaloclastic or tuffaceous).
8. A description of the alteration: fresh (<2% alteration products), slightly altered (2%–10%), moderately altered (10%–40%), highly altered (40%–80%), very highly altered (80%–95%), or completely altered (95%–100%). Changes of alteration through a section or a unit were also noted. Additional detailed descriptions of alteration and weathering of igneous units are reported in "Alteration," p. 6.
9. A description of veins and fractures, including their abundance, width, mineral linings and fillings, and, where possible, their orientation. Additional detailed descriptions of vein materials are reported in "Alteration," p. 6.
10. Additional comments, including notes on the variability of the unit.

Rock Classification

Volcanic rocks were classified according to the nature and abundance of phenocryst assemblages. The rocks were described as aphyric when 1% phenocrysts were visible with a hand lens or under a binocular microscope. Porphyritic volcanic rocks were further classified by phenocryst type using mineral name modifiers given in the order of decreasing abundance. Given the predominance of cryptocrystalline to microcrystalline quench crystal morphologies in the groundmass of most rocks recovered during Leg 187, the term "phenocryst" was used for a crystal that was significantly larger than the average size of the groundmass crystals; in practice, these were generally >~1 mm. Thus, a "highly olivine-plagioclase phyric basalt" contains >10% phenocrysts, the dominant phenocryst being olivine, with lesser amounts of plagioclase. The prefix includes all of the phenocryst phases that occur in the rock, as long as the total content >1%. Rock names were assigned initially on the basis of hand-specimen observations and later were checked with the thin sections. The term "glass" was reserved for a homogeneous, isotropic material free of quench crystals, with <2% alteration. Altered or hydrated glass was designated palagonite. In chilled margins, glass containing discrete spherulitic quench growth was distinguished from clear glass free of these textures.

Designation of Lithologic Units

The core was subdivided into consecutively numbered lithologic units. Lithologic unit boundaries were generally defined on the basis of major changes in lithology (i.e., changes in phenocryst type or content and/or texture). Boundaries were placed at the lowest piece of the upper interval. Generally, boundaries were not defined on the basis of type or degree of alteration or deformation. Lithologic units defined as rubble, breccia, or talus may consist of more than one rock type; such units were generally identified by the random mixture of lithologic types in

the core, a predominance of weathered rounded surfaces and/or cementing sediments (i.e., breccias).

Thin-Section Descriptions

Thin sections from most igneous-rock units recovered during Leg 187 were examined to complement the hand-specimen observations. Specifically, thin sections were used to (1) confirm the rock name assigned from macroscopic description of the core and (2) determine alteration mineralogy. Features of the thin sections described included

1. Texture, mineral type, morphology, abundance, overgrowths, zoning, and twinning;
2. Accessory minerals (e.g., Fe-Ti oxides and sulfides) and inclusions;
3. Xenocrysts; and
4. Secondary mineral type, morphology, and abundance, including vein, vesicle, and fracture fillings.

Modal data were visually estimated by reference to standard charts. Crystal sizes were measured using a micrometer scale; generally, these measurements are more precise than hand-specimen estimates. Groundmass textural terms used are listed in Table T1. All data are summarized in ODP format thin-section description forms (see the "Core Descriptions" contents list for thin-section information for each site).

T1. Groundmass textural terms, p. 33.

ALTERATION

Many igneous rocks recovered during Leg 187 have undergone secondary alteration in a deep marine environment. In these descriptions alteration is defined as the chemical transformation of mineral assemblages due to the percolation of fluids. On the HRVCD forms, rocks are graded according to whether they are fresh (<2% by volume alteration/weathering products) or have slight (2%–10%), moderate (10%–40%), high (40%–80%), pervasive (80%–95%), or complete (95%–100%) alteration. We described the types, forms, and distributions of secondary alteration as well as abundances of vesicles and their mineral fillings and veins. Any changes in alteration styles throughout a section or an igneous unit are also recorded on the HRVCD form.

Alteration of cores was described on a piece-by-piece basis. Descriptions are based mostly on hand-specimen observations; specific clay, zeolite, and carbonate minerals are not generally distinguished, except where crystal morphology allows unequivocal identification. Where additional mineralogical evidence is available from either thin-section descriptions and/or X-ray diffractograms, these identifications were integrated into the HRVCDs. Where appropriate, hand-specimen descriptions were augmented with thin-section observations.

MICROBIOLOGY

The primary microbiology objective for Leg 187 was to determine the diversity and habitat of microbes in igneous rocks of different ages and to identify and quantify microbes participating in the alteration of the basalt. To achieve these objectives, samples of pillow lavas and other

lava flows were collected from the cores for cultivation experiments, for later onshore characterization of DNA contained within them, and for examination of extant and fossil microbial activity by electron microscope techniques. Some sediment samples were also collected for cultivation and DNA analysis. The shore-based studies will be performed at the University of Bergen, Norway, and at Japan Marine Science and Technology Center (high-pressure cultivation).

Interpretation of results is complicated by the possibility of contamination of samples with microbes from the seawater (used as drilling fluid), the ship and drilling equipment, and from postcollection processing of samples. To determine the extent of microbial contamination during drilling, surface seawater was sampled to characterize DNA, and downhole tracer tests were conducted. A sample handling protocol was established to minimize postcollection contamination.

Igneous Rocks

Sampling

Whole-round cores were collected on the catwalk through the ends of unsplit core liners or in the core splitting room immediately after the core liner was split. The cores were handled only with latex gloves washed with 70% ethanol. Two approaches to minimize drilling-induced contamination of the outer rock sample surfaces were followed. The outer surface was either quickly flamed with an acetylene torch, or it was split off using a hydraulic rock trimmer. Flaming proved to be the simplest and fastest method, which minimized the time the rock samples were exposed to oxygen. After the sterilization, the samples were split into pieces of suitable size. Samples for enrichment cultures were placed in sterile plastic bags inside cold glass flasks containing 5 mL of seawater to keep them moist; these samples were immediately refrigerated (~5°C). Samples for anaerobic enrichment were placed in nitrogen-flushed flasks. The samples were contained in anaerobic and cold conditions within 20–30 min of the core arriving on deck.

Pieces of core, kept moist with 1 mL of anaerobic or aerobic seawater, were gently crushed into smaller grains in a sterile percussion mortar. For anaerobic enrichment this was done inside an anaerobic glove bag (Instruments for Research and Industry, model S30-20) flushed with a mixture of N_2 (90%), H_2 (5%), and CO_2 (5%). Additional pieces of core were used whole as described below.

Enrichment Cultures

Fourteen types of bacterial culture media—11 anaerobic and 3 aerobic—were used to try to enrich viable microbial populations from the rock samples. The media were based on the composition of seawater and were contained in airtight 10-mL serum bottles. The anaerobic media were reduced with sulfide, and Mn(IV), Fe(III), sulfate, or bicarbonate were added as electron acceptors. For the aerobic media, oxygen was the electron acceptor. Electron donors were organic carbon sources (formate, acetate, lactate, succinate, glucose, yeast extract, trimethylamine, and peptone), hydrogen, and methane. Approximately 1 g (0.25–0.5 cm^3) of crushed rock was added to each type of culture medium.

In addition, 4–5 g of crushed rock was added to two types of microcosm in 250-mL flasks filled with 200 mL anaerobic seawater. One contained Mn(II) as an added electron acceptor and the other contained

Fe(II) and sulfate. Chitin, pectin, and acetate were added to both types as carbon sources. This setup is designed to establish a gradient from anaerobic conditions at the bottom of the flask to aerobic conditions at the top, with a micro-aerobic intersection in between. Enrichment of bacteria participating in the manganese-, iron-, and sulfur-redox cycles was the aim of these microcosm experiments, where the elements will be reduced in the anaerobic zone and oxidized in the aerobic zone of the flask. All samples were incubated at ~5°C. Growth is confirmed by the accumulation of metabolic products and of microbial cells. Finally, 5–10 g of sample was immediately frozen and stored at –70°C for high-pressure cultivation.

Molecular Biology Analysis

Three approaches were used for cell recovery from the rocks for later DNA analysis. First, a phosphate-buffered saline (PBS) solution of NaH_2PO_4 (2 mM), Na_2HPO_4 (8 mM), and NaCl (130 mM), which had a pH of 7.2, was applied to wash cells off fracture surfaces in the samples. This potential cell suspension was immediately frozen at –70°C.

Second, samples were crushed in a mortar filled with PBS. After some settling, the PBS was collected and centrifuged at 4000 rpm for 20 min. The supernatant was then discarded, and the potential cell pellet was frozen at –70°C. These samples were frozen for shore-based analysis.

Third, pieces of rock (1–2 cm^3) were fixed with 70% ethanol in sterile 15-mL Falcon plastic tubes for onshore in situ hybridization.

Electron Microscope Techniques

Samples from both glassy margins and crystalline interiors of lava flows and pillows were collected for shore-based examination of extant and fossil microbial activity by electron microscope techniques. Some of the samples were subsamples of those collected for microbial cultivation and DNA extraction. The samples were either air dried or preserved in artificial seawater containing 2% glutaraldehyde.

Sediments

Sediment samples taken from the interiors of the cores using sterile spatulas and spoons were immediately placed in sterile plastic bags inside cold, anaerobic flasks. The sediment samples (~1 g) were inoculated inside the anaerobic glove bag using the same 10 anaerobic and 3 aerobic media as described for the igneous rock samples. No microcosms were prepared with sediment inoculum.

For shore-based DNA analysis, sediment samples were fixed in 70% ethanol in sterile 15-mL Falcon plastic tubes and stored at 5°C.

Surface Seawater

Surface seawater samples were collected using a flask lowered from the bow of the ship to avoid wastewater and cooling water from the ship. One aliquot of the seawater samples was immediately fixed by adding ethanol to a final concentration of 40%. The ethanol-fixed seawater was later filtered for enumeration of microbes. A second aliquot was centrifuged (4000 rpm, 20 min) to separate seawater supernatant from a residual cell pellet. The cell pellet was washed with PBS and then

frozen at –70°C. The cell pellet will be used for shore-based DNA analysis.

Tracer Test

To determine potential levels of contamination of samples during drilling, we used yellow-green fluorescent carboxylate microspheres (Polysciences, Inc.) 0.518 µm (±0.021 µm) in diameter as a particulate tracer. These microspheres show bright green fluorescence when observed under epifluorescence microscopy using a blue filter set. To achieve an approximate concentration of 10^{10} microspheres/mL, 2 mL of the microsphere suspension (2.86% solids in deionized water) was diluted to 40 mL with distilled water. This diluted solution was placed in an ultrasonic bath to disrupt aggregates. The diluted solution was poured into a plastic bag, excess air was expelled, and the bag was heat sealed and wedged into a recess in the top of an auxiliary core-catcher insert supported by the core-catcher fingers. The first core to enter the barrel ruptures the bag, dispersing the microspheres into the core barrel.

After splitting the core liner, pieces of rock close to the top of the core were selected to maximize the probability of finding the microspheres. The surface of the rock was washed with distilled water, and aliquots of the wash water were filtered onto polycarbonate filters. Rock thin sections were then prepared with no special precautions. For sediment cores, smear slides were made from both the outer surface and interior of the core using nonfluorescent immersion oil (Olympus). A Zeiss Axiophot epifluorescence microscope with a 100W mercury lamp, a blue filter set, and a 100× Plan-Neofluar oil-immersion objective was used to check for presence of microspheres.

STRUCTURAL GEOLOGY

Structural features in the cores recovered during Leg 187 are summarized on the HRVCDs. For each section, more detailed structural information, such as the apparent and true orientations of veins and fractures and crosscutting relationships, is described and sketched on a separate structural geology description form (e.g., Fig. **F4**). With reference to the structural geology checklist (Table **T2**), observations are recorded to a structural log spreadsheet (Fig. **F5**) (see the **"Supplementary Materials"** contents list).

Descriptions and structural measurements were based on observations of the working half of the core. We followed the procedures used for the description of hard rocks in the "Explanatory Notes" chapter of the Leg 153 *Initial Reports* volume (see Cannat, Karson, Miller, et al., 1995).

All the structural features were recorded (in centimeters) relative to core-section depths from the top of the core section. Depth is defined as the point at which the structure intersects the center of the cut face of the working half of the core, as detailed in figure 15A in Cannat, Karson, Miller, et al. (1995).

Apparent fault displacements were recorded as they appear on the cut face of the archive half of the core and the ends of broken pieces. Displacements seen on the core face were treated as components of dip-slip movement, either normal or reverse. Displacements of features visible on the upper and lower surfaces of core pieces were treated as com-

F4. Structural geology description form, p. 26.

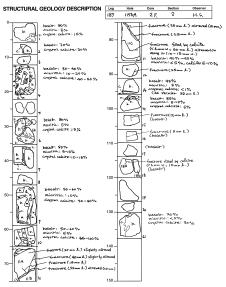

T2. Structural geology checklist, p. 34.

F5. Structural geology log, p. 27.

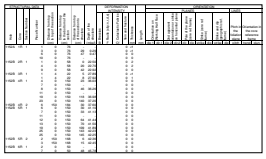

ponents of strike slip and termed sinistral or dextral. Displacements were measured parallel to the trace of the fault between displaced planar markers. Additional cuts and slickenside orientations were incorporated wherever possible to differentiate between apparent dip-slip, oblique-slip, and strike-slip displacements.

Structures were oriented using the techniques outlined during Legs 131 (Taira, Hill, Firth, et al., 1991) and 153 (Cannat, Karson, Miller, et al., 1995). Our assumption is that the core axis is always vertical within a horizontal slice of the core. Pseudonorth (000°) is defined as 90° to the cut face of the archive core; the right side is designated 270° and the left side is 090° (Fig. F6).

F6. Convention used to orient structures, p. 28.

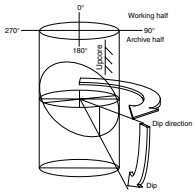

UNDERWAY GEOPHYSICS

Underway geophysical data were collected during all transits. To reconfirm the position of a proposed drill site, a short single-channel seismic (SCS) survey was conducted on the approach to most sites during Leg 187. Onboard instrumentation used included a precision echo sounder (3.5 kHz), gyrocompass (Lehmkul LR40), seismic survey system, and Global Positioning Systems (GPSs).

Navigation

Throughout Leg 187, three GPS units were available, with output provided to the Underway Geophysics Laboratory. The Ashtech GG24 system was the primary navigation device. Older Omnistar and Magnavox systems were not used.

GPS fixes were available continuously (1-s updates) and recorded at 60-s intervals. Event data were recorded at 60-s intervals on site and in transit. Navigation data were logged by the WinFrog software system, which was installed on a dedicated personal computer in the Underway Geophysics Laboratory. Subsequent processing and display of navigation data were performed using the Generic Mapping Tools (GMT) software package (Wessel and Smith, 1995) on shipboard UNIX workstations.

Echo Sounders

Both 3.5- and 12-kHz echo sounders (precision depth recorders [PDRs]) were used to acquire bathymetric data as well as high-resolution reflection records of the uppermost sediment layers. Although the resolution of 12-kHz data is higher than that of 3.5-kHz data, the 12-kHz PDR has little penetration ability in these water depths. Data were recorded on two EPC 8082 analog line-scanning recorders at 3.5 and 12 kHz, respectively. The 3.5-kHz system used a Raytheon CESP III correlator echo sounder processor driven by a Raytheon PTR105B transceiver with a 2-kW sonar transmitter. This system included a single EDO-Western type 323c transducer mounted in a sonar dome on the hull 40 m forward of the center of the moonpool. This location was chosen to reduce ship-generated noise and signal attenuation from aeration beneath the hull. The recorder annotated automatically at fixed intervals; ship speed and heading were marked every 5 min and position every 30 min. Depth readings were taken manually at 5-min intervals and entered into an Excel spreadsheet.

Seismic Reflection Profiling

The SCS data were received using a single-channel Teledyne model 178 hydrophone streamer with a 100-m-long active section containing 60 hydrophones, a 25-m-long "stretch" section, and a 150-m lead section. The gun and streamer were both towed at 12–18 m depth. Ship speed was kept at ~5.5 kt during all seismic surveys. One 80-in^3 water-gun source operated at 2000 psi and was triggered from the WinFrog navigation system at a shot interval of 12 s, equivalent to ~33 m at 5.5 kt. The gun was towed ~20 m astern. Analog data were recorded on one Raytheon model 1807M recorder, displaying scan intervals of 4–12 s and band-pass filtered from 30 to 100 Hz throughout the seismic survey. A Krohn-Hite model 3550 analog filter was used to filter signals to the recorder.

The seismic data from each shot were sampled every 1 ms from 0 to 8 s and were digitally recorded on a Sun Sparcstation 10 in SEGY format, using the "a2d" acquisition package after applying an anti-aliasing filter with a corner frequency of 250 Hz. Seismic data were copied to both 4- and 8-mm digital audiotapes during the site survey and then processed using the SIOSEIS software package (Paul Henkart, Scripps Institute of Oceanography) and displayed on a HP 650C Design Jet plotter. Processing of SCS water-gun data acquired during Leg 187 included water-bottom mute, band-pass filter (25–120 Hz), automatic gain control using a 500-ms window, and removal of every other trace.

SEDIMENT DESCRIPTION

The description of sediments recovered during Leg 187 includes brief macroscopic core descriptions including grain size, lithology, drilling disturbance, color, and estimates of sediment composition based on smear slides. These data were recorded in the shipboard electronic core description archive AppleCORE (version 0.7.5g) using ODP standard nomenclature and symbols throughout.

Barrel Sheet Data

AppleCORE generated a one-page graphic log (barrel sheet) of each core. Barrel sheets are presented with electronic links to core photographs (see the "**Core Descriptions**" contents list). For Leg 187, grain size was recorded as a strip log, lithologies are represented by graphic lithology patterns, and deformation and disturbance of sediment that resulted from the coring process are illustrated in the "Drilling Disturbance" column, according to ODP convention. Blank regions in this column indicate the absence of visible drilling disturbance. Smear-slide locations are also given on the barrel sheets. Color was determined where distinct color changes were observed using a handheld Minolta CM-2002 spectrophotometer and translated to text terms using standard Munsell color charts (Munsell Color Company, Inc., 1975; Rock-Color Chart Committee, 1991). A summary of the sedimentologic observations is given in the "Description" column of the barrel sheet. It consists of a heading in capital letters that lists only the dominant lithologies and a general description of the sediments, including color, composition, and any other general features of note.

GEOCHEMISTRY

Introduction

A key element of ODP Leg 187 was the use of onboard geochemical analysis in support of the primary leg objective—to locate and characterize the boundary between isotopically defined Indian-type and Pacific-type mid-ocean-ridge basalt (MORB) mantle provinces between Australia and Antarctica. First recognized along the Southeast Indian Ridge (SEIR) (Klein et al., 1988), the isotopic boundary is now known to have migrated westward in the last 4–5 m.y., based on analyses of 0- to 7-Ma off-axis dredge samples (Pyle et al., 1992; Christie et al., 1998). Although the boundary is defined by the isotopic signatures of seafloor lavas (assumed to represent the mantle source), examination of SEIR MORB glass data from this region has shown that the great majority of 0- to 7-Ma lavas can be correctly identified as Indian or Pacific type based on variations in Ba and Zr contents (Fig. F7) (Pyle et al., 1995; D.G. Pyle and D.M. Christie, unpubl. data).

From 0 to 4 Ma, the isotopically defined mantle boundary coincides with a distinct morphological change in seafloor fabric. The seafloor to the east (Pacific side) of the boundary is characterized by smooth, ridge-parallel abyssal hills, whereas rough, highly tectonized, chaotic terrain occurs to the west (Indian side) (Christie et al., 1998). The change between smooth and rough seafloor topography is inferred to reflect contrasts in melting conditions and magma supply within a segment. Differentiation trends of lavas dredged from these two types of seafloor terrain are distinct enough to be recognized on simple Mg-oxide variation diagrams (Figs. F8, F9). We therefore have two means of delineating the isotopic boundary: (1) by a mantle source geochemical signature and (2) by compositional indicators of mantle melting conditions that also influence axial morphology and, consequently, seafloor fabric. For shipboard use, we chose the diagram of each type that best discriminated 0- to 7-Ma Indian from Pacific lavas. These are Zr/Ba values vs. Ba content and Na_2O/TiO_2 vs. MgO.

For every site, we have prepared a geochemical summary that includes

1. A table of major and trace element concentrations determined by inductively coupled plasma–atomic emission spectrometry (ICP-AES) and by XRF;
2. An overview of the basalt compositional range within each hole and its relation to macroscopically and microscopically identified lithologic units;
3. A comparison of glass and whole-rock compositions; and
4. A comparison of XRF and ICP-AES results for individual whole-rock samples.

The glass data are then compared with dredged 0- to 7-Ma lavas from the SEIR segment in which the site is located. Figures F8 and F9 show major and trace element MgO variation diagrams for 0- to 7-Ma MORB from the SEIR between 123°E and 133°E. These MORB glass data provide the basis for site-by-site comparison, allowing an evaluation of whether the mantle source and/or melting characteristics within individual segments have changed through time.

F7. Variations in Zr/Ba vs. Ba of basaltic glass and in Na_2O/TiO_2 vs. MgO of basaltic glass, p. 29.

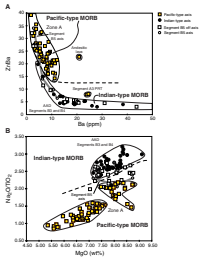

F8. Major element variations vs. MgO for 0- to 7-Ma lavas between 123°E and 133°E, p. 30.

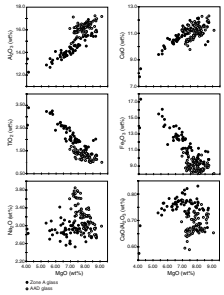

F9. Trace element variations vs. MgO for 0- to 7-Ma lavas between 123°E and 133°E, p. 31.

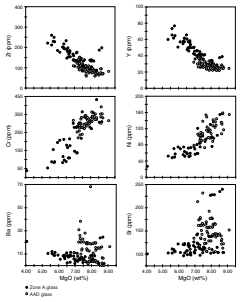

Finally, the mantle province for basalts at each site is assessed based on variations in Zr/Ba vs. Ba and Na_2O/TiO_2 vs. MgO (Fig. **F7A, F7B**). The basis for using Zr/Ba vs. Ba to discriminate between Pacific-type and Indian-type isotopic mantle provinces is shown in Figure **F10A** and **F10B.** Isotopically, $^{206}Pb/^{204}Pb$ clearly defines a sharp boundary between Indian-type (<18.3 $^{206}Pb/^{204}Pb$) and Pacific-type (>18.5 $^{206}Pb/^{204}Pb$) MORB mantle sources along the SEIR at ~126°E (Pyle et al., 1992; Pyle et al., 1995). The Zr/Ba values show a positive correlation with $^{206}Pb/^{204}Pb$ and separate the Indian type from the Pacific type with little overlap. Most Indian-type MORBs have Zr/Ba values <14, and most Pacific-type MORBs have Zr/Ba values >14. A few samples cannot be distinguished by Zr/Ba values alone; for these, Indian- and Pacific-type MORBs can usually be distinguished, as they have slightly different Ba concentrations for a given Zr/Ba ratio (Fig. **F7A**).

Although Ba seems an unlikely geochemical discriminant because of its susceptibility to contamination by seawater, particularly in older seafloor basalts, it is the only choice, given the analytical limitations of seagoing instrumentation. We relied on fresh basaltic glass, free of alteration, for this assessment throughout Leg 187 because whole-rock crystalline interiors are clearly prone to seawater circulation and alteration. This can be seen in many of the whole-rock analyses, which tend to have higher Ba contents than associated basaltic glasses. Nevertheless, as data accumulated through the leg, it was apparent that whole-rock data formed coherent trends with their associated glasses at most holes. For Indian samples, these glass–whole-rock trends lie at lower Ba values for a given Zr/Ba than for Pacific samples (see Fig. **23A,** p. 35, in the "Site 1156" chapter and the individual site chapters for details).

F10. A. Variations in $^{206}Pb/^{204}Pb$ and in Zr/Ba vs. $^{206}Pb/^{204}Pb$ in SEIR lavas dredged from 0- to 7-Ma seafloor, p. 32.

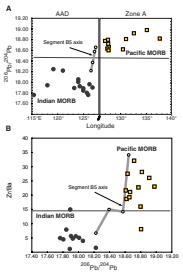

Analytical Procedures

Introduction

The data set for each site includes major and trace element data from both standard ODP XRF and newly developed (for ODP) ICP-AES analytical procedures. Elements analyzed by XRF include Si, Ti, Al, Fe, Mn, Mg, Ca, Na, K, P, Nb, Zr, Y, Sr, Rb, Zn, Cu, Ni, Cr, V, and Ce. Elements analyzed by ICP-AES include Si, Ti, Al, Fe, Mn, Mg, Ca, Na, K, P, Zr, Y, Sr, Ba, Ni, Cr, and Sc. The Zn, Cu, and V contents of typical MORBs are well within the analytical capabilities of the ICP-AES, but these trace elements were omitted from the analytical routine to minimize Ar usage, an important consideration at sea. Data tables for each site report include

1. The XRF major element analysis of each of two fused disks per sample;
2. The XRF trace element analyses of a single pressed-powder pellet per sample (both disks and the pellet are made from splits of a single sample powder);
3. ICP-AES major and trace element analyses of splits of the XRF whole-rock powders; and
4. ICP-AES analysis of handpicked glass chips.

Unless otherwise indicated, ICP-AES analyses presented in duplicate represent separate analyses of a single sample dissolution. Where dupli-

cate analyses are presented in the tables, the geochemical variation diagrams show only the averaged values.

Our first analytical priority was to quickly determine the probable mantle source (Indian or Pacific type) by analyzing picked, fresh glass in order to facilitate drilling target selection. The ability to accurately analyze Ba and Zr (e.g., ±1 ppm Ba in the range of <5–10 ppm) enabled us to select the next site based on rapid analyses of samples recovered at an occupied site. This was critical to our responsive planning and enabled a much more precise tracing of the mantle boundary than would have been possible otherwise. Our second priority was to characterize the compositional variability of each hole by analysis of representative samples from lithologic units identified in hand sample and thin section.

X-Ray Fluorescence Analysis

Representative samples of major lithologic units were selected for shipboard XRF analysis. Large pieces (~20 cm^3) were reduced to fragments <1 cm in diameter by crushing between two disks of Delrin plastic in a hydraulic press. The sample was then ground for ~5 min in a Spex 8510 shatterbox with a tungsten carbide barrel. Contamination of the samples with Nb during grinding was investigated prior to the start of Leg 152, and none was detected (Larsen, Saunders, Clift, et al., 1994).

Major elements were analyzed using fused lithium tetraborate glass disks doped with lanthanum oxide as a heavy absorber (Norrish and Hutton, 1969). The disks were prepared from 600 mg of rock powder that had been ignited for 2 hr at about 1025°C and mixed with 7.2 g of dry flux consisting of 80% lithium tetraborate and 20% lanthanum oxide. This mixture, with 20 mL of lithium bromide (8.6 M) added to prevent adhesion to the Pt-Au crucible, was melted in air at 1150°C for ~4 min with constant agitation to ensure thorough mixing and then cooled. Trace elements were analyzed using pressed-powder pellets. These were made by mixing 5 g of rock powder with 30 drops of a solution of Chemplex polymer in methylene chloride (100 mg/cm^3) and then pressing the mixture into an aluminum cap under a load of 8 T. We measured loss on ignition from weighed powders heated for 4 hr at 1025°C.

A fully automated wavelength-dispersive ARL 8420 XRF system (equipped with a 3-kW generator and a Rh-anode X-ray tube) was used to determine the major and trace element concentrations in the samples. With the 12:1 flux:sample ratio and the use of the heavy absorber, matrix effects within the fused glass disks are insignificant over the normal range of igneous rock compositions, and the relationship between X-ray intensity and element concentration is linear. A pressed pellet made with 5 g of basalt powder should be infinitely thick at the shortest wavelengths used in the analysis. X-ray intensities were corrected for line overlap and interelement absorption effects. The latter corrections were based on the relationship between mass absorption coefficient and the intensity of the Rh-Ka Compton scatter line (Reynolds, 1963, 1967; Walker, 1973). Analytical conditions are given in Table **T3.** The spectrometer was calibrated using a suite of 30 well-analyzed reference standards. Standard values recommended by Govindaraju (1989) were used for all elements. Precision estimates, based on replicate shipboard analyses of reference standards AII-92, MGR-1, and BIR-1, are given in Table **T4** (major elements) and Table **T5** (trace elements).

T3. XRF operating conditions during analyses, p. 35.

T4. XRF major element analytical accuracy, p. 36.

T5. XRF trace element analytical accuracy, p. 37.

Inductively Coupled Plasma–Atomic Emission Spectrometry

Major and trace element concentrations of both glass and whole-rock samples were determined with the JY2000 ULTRACE ICP-AES that was installed aboard the *JOIDES Resolution* immediately prior to Leg 187. ICP-AES protocols were developed by R. Murray (unpubl. data) and optimized by Leg 187 shipboard technical staff and scientists for the rapid dissolution and analysis of basaltic glass chips and whole-rock powders. The ICP-AES methods and procedures that we tested and adopted are described below in detail. The ICP-AES offers several advantages over routine XRF analysis in that

1. Samples can be recovered, processed, and analyzed in <12 hr;
2. Sample size is considerably less than that required by XRF; major and trace element analyses can be completed on a single 100-mg sample;
3. Weighing time is cut in half (fewer weighings are required, and the smaller sample weights can be determined more rapidly);
4. The detection limits for certain trace elements, particularly Ba, are superior to those for XRF.

Most samples analyzed by XRF during Leg 187 were duplicated by ICP-AES as a quality control check because the JY2000 ICP-AES is a new seagoing analytical tool. Overall, the major and trace element data agree within the error of each analytical method.

Because the ICP-AES was a new analytical instrument, considerable technique development occurred in the early weeks of Leg 187. During this time, samples were analyzed under a variety of instrument conditions. The specific analytical conditions for each sample run are provided in Table **T6.** ICP-AES analyses of samples from the first three sites are of questionable quality; glass samples were reanalyzed later in the leg. Sample runs containing data of questionable quality are noted below and in the site chapters.

T6. ICP-AES operating conditions and sample run parameters, p. 38.

Details of the ICP-AES Analytical Procedure

Analytical Setup

The JY2000 is a sequential atomic emission spectrometer that measures the intensities of characteristic emission wavelengths between ~100 and ~800 nm, one peak at a time. Therefore, analysis time depends on the number of elements determined, the number of emission lines per element, the mode of analysis, the number of replicates, and the counting time. The 18 elements analyzed during Leg 187 and the emission lines used are listed in Table **T7.** All ICP-AES data presented in the site chapter reports were analyzed using Mode 5 (see **"Mode of Analysis,"** p. 19) of the JY software. With this analytical mode, the intensity at the peak of an emission line is measured and averaged over a 1-s (2 s for Ni, Cr, Na, and K) counting interval repeated three times (see **"Mode of Analysis,"** p. 19). Each sample solution was repeated at least once during a single run, except in sample runs Leg187B and Leg187C. Major and trace elements were measured during a single run using the autoattenuation feature of the JY2000 software, which adjusts the photomultiplier voltage to optimize the peak to background ratios for each emission line.

T7. Element emission lines for ICP-AES analyses, p. 39.

Our analytical and sample preparation techniques were significantly improved by the time we arrived at Site 1155 (sample run Leg187D; Table T6), resulting in greater plasma stability, thus greatly reducing signal noise. Both V-groove and concentric nebulizers were tested. Filtering of solutions and higher sample dilutions are required for the concentric nebulizer. We preferred the concentric nebulizer since it delivers a finer, more stable aerosol to the plasma, resulting in a more stable signal (see Table T6). Greater sample dilution also reduces salt buildup on the torch glassware.

Initial Analytical Tuning

The mechanical step position of each emission line was initially calibrated using 10-ppm single-element standard solutions prepared at Boston University. We did not have a single-element Sc solution aboard, so we calibrated the emission peak closest to the theoretical step position of Sc (361.84 nm) using a solution of the Lamont-Doherty Earth Observatory rock standard K-1919. Multielement standards approximating typical basalt concentrations were prepared in 10% HNO_3 and used during the first 2 weeks of the leg to check the initial-emission-line calibration by autosearching a small (0.002 nm) window across each emission peak. A second tuning of emission line positions was then performed by again autosearching a small (0.002 nm) window using the K-1919 basalt-rock standard. A peak profile was collected for each emission line during the initial setup by using the K-1919 standard to determine peak-to-background intensities and to set the locations of background points for each element. To optimize peak to background conditions, the photomultiplier was set for each element by autoattenuating on the K-1919 standard.

Sample Preparation

At sites where rapid decisions were needed, the first recovery of basaltic glass was sampled for immediate processing. Additional samples were selected based on availability of glass, position in the core, and number of units defined. Glass samples were chipped from whole-rock pieces by hammering the sample while it was wrapped in plastic-coated freezer paper or, alternatively, by chiseling. The resulting mixed whole-rock and glass-chip product was then carefully crushed in an alumina mortar and pestle, sieved to a 1- to 2-mm fraction, washed and insonified in nanopure H_2O for 20–40 min (depending on the extent of palagonite alteration), and dried in an oven at 80°–100°C. Fresh shiny black basalt glass was then hand-separated from all altered material, minerals, whole-rock chips, and spherulitic microcrystalline material, under binocular magnification.

We weighed 0.100 ± 0.002 g of glass chips or whole-rock powder (prepared for XRF) and mixed it with 0.400 ± 0.0004 g of Li-metaborate ($LiBO_2$) flux that was preweighed onshore. Standard rock powders and full procedural blanks were included with the glass and whole-rock unknowns for each sample run. For Sites 1152 and 1153, standard powders were preignited at 1025°C for 4 hr before weighing and fusing. After Site 1153 (sample run Leg187C) only unignited standards were used since glass and whole-rock unknowns were never preignited prior to weighing for ICP-AES analysis. Samples and standards were weighed on a Cahn automatic electrobalance attached to a gimballed table. Weighing errors at a 99.5% confidence are conservatively estimated to

be ~±0.0001 g. Weighing a single sample can take as long as 15 min on station in moderate seas, even though the low inertial forces applied to the balance by small sample weights help to speed the weighing process. This and handpicking of difficult glass samples were the time-limiting steps in the analytical process. Minimum sample processing time for ICP-AES (from on deck to dissolution) is ~5–12 hr.

Rock powder/flux mixtures were fused in Pt crucibles heated by the same induction furnace apparatus used for XRF glass-bead preparation. A lithium bromide wetting agent was used to prevent the cooled bead from sticking to the crucible. Cooled beads were transferred to 60-mL wide-mouth Nalgene polypropylene bottles and dissolved in 50 mL of 5% HNO_3 by shaking with a Burrell Wrist Action bottle shaker for ~1.5 hr. After digestion of the glass bead, 10 mL of this solution was passed through a 0.45-µm filter and diluted with 30 mL of 5% HNO_3. Each sample and standard solution was spiked with 5 ppm Ge as an instrument drift monitor. The final solution-to-sample dilution factor for this procedure is ~2000.

Routine Analytical Procedure

The JY2000 plasma was ignited 30 min before each run to warm up and stabilize the instrument. After the warm-up period, the following steps are required: (1) a zero-order search required by the software is carried out to check the mechanical zero of the diffraction grating; (2) the mechanical step positions of the emission lines are tuned by autosearching a small (0.002 nm) window across each emission peak using a K-1919 standard solution; (3) autoattenuation is performed using the K-1919 standard if there have been significant changes in operating conditions, such as changing the nebulizer.

A typical sample run (see **"Sample Run Format and Data Reduction,"** p. 17) lasts from 4 to 6 hr, depending on the number of samples and the number of sample repeats. Each run used 50%–75% of a high-pressure Ar bottle.

Sample Run Format and Data Reduction

A typical ICP-AES run consisted of

1. Five rock standards, including both certified United States Geological Survey (USGS) rock standards and well-characterized in-house laboratory rock standards (Table T8). These standards were run at the beginning, the end, and one or more times during each sample run;
2. Six to eight glass and/or whole-rock samples;
3. The USGS standard, BHVO-2, and the Zone A dredged whole-rock sample MW8801-17-26 were run as unknowns in every sample batch in order to monitor analytical accuracy and reproducibility;
4. A drift-correcting sample (the K-1919 standard) was run at every fifth sample position; and
5. A blank solution was run at the beginning and end of each run.

Instrument stability and short-term drift was monitored with the ~5-ppm Ge internal spike added to each solution. Lithium is also useful as an instrument drift monitor since each sample was fused with approximately the same amount of $LiBO_2$ (e.g., Ramsey et al., 1995).

T8. Major and trace element values for ICP-AES standard curve calibrations, p. 40.

Following each sample run, the raw intensities were transferred to a data file, and data reduction was completed by spreadsheet to assure control over standardization and drift correction (we did not test the instrument's data reduction software): (1) intensities for all samples were corrected by subtracting the procedural blank; (2) drift correction was accomplished by interpolating between two consecutive drift-correcting solutions and normalizing the intensities of the intervening samples; (3) normalized intensities were corrected for sample weight; and (4) concentrations were determined using calibration curves created from replicate measurements of the USGS and in-house standards (Table T8).

ICP-AES Accuracy and Reproducibility

Estimates of accuracy and precision for major and trace element analyses are based on replicate analysis of the USGS reference standard, BHVO-2, and the Zone A SEIR whole-rock basalt sample MW8801-17-26 (Tables T9, T10). In general, replicate analyses of BHVO-2 are accurate to within 3% for major elements and 5% for trace elements. For most elements, shipboard analyses of BHVO-2 by ICP-AES are slightly lower than published values but well within the analytical error reported by Plumlee (1998a, 1998b) (Tables T9, T10). Within-run precision of replicates improved greatly during the course of Leg 187, to much better than 3% for most elements. Run-to-run precision was <3% for the major elements, with the exception of K, Na, and P. Na and K have poorer precision because of the instability of the sheath gas flow (see "Plasma Instability," p. 19). Run-to-run precision for trace elements was <5%, depending in part on the concentration of the element in the sample. For example, compare the relative standard deviation (RSD) and Ba values for MW8801-17-26 and BHVO-2 in Table T10.

In general, the ICP-AES and XRF analyses compare very well (see the "Geochemistry" sections in the individual site chapters), except for Ni and Cr, which were consistently lower in the ICP-AES analyses. XRF Cr results are consistently high relative to published standards values, and Ni tends to be low. The ICP-AES Ni and Cr data are problematic as well (see Fig. F9).

T9. Accuracy estimates for ICP-AES major element analyses, p. 41.

T10. Accuracy estimates for ICP-AES trace element analyses, p. 42.

ICP-AES, Method Development, and Problems and Solutions

Sample Digestion Problems

Before developing the successful technique described above, several problems compromised the quality of the data from early sample runs.

The concentration of the digestion acid was based on tests with 1%, 2%, 5%, and 10% HNO_3. We determined that a cooled, fused bead dissolved in 50 mL of 5% HNO_3 in a heated ultrasonic bath within ~60 min. Sample solutions were not diluted further for our initial ICP-AES runs because many trace elements were at or near their detection limits. We encountered significant problems with Si gel formation when dissolving samples in bottles in a heated ultrasonic bath. The gel problem was clearly observed by using clear 50-mL polypropylene Corning centrifuge tubes. These tubes are highly recommended because they allow a visual check on undissolved particulates and/or the formation of Si gel. Si gel formation was the dominant cause of our initial poor results,

affecting runs Leg187A and B. Gel formation is promoted if a compositional gradient is allowed to develop in the dissolution vessel; this is a severe problem with stationary bottles in an ultrasonic bath but is readily avoided by using a mechanical shaker. We used a shaker for the remainder of Leg 187 with no further gel-formation problems.

By sample run Leg187D, we determined that plasma stability and analytical accuracy improved if samples were filtered and significantly more diluted, at least ~2000 times. The additional dilution did not compromise detection limits as it allowed the use of the concentric nebulizer, increasing the efficiency of sample aspiration.

Mode of Analysis

Five modes of analysis are available in the JY software. During the first week of Leg 187, the total analysis time and counting statistics of three of these modes were briefly compared: Mode 1 measures intensities at a variable number of points (3–11) across a peak and then averages the intensities of a subset (1–9) of those points with the largest intensities. For example, Mode 1 will average the intensities of the three highest contiguous "points" within a set window that can include as many as 11 preset positions across a peak. Mode 2 fits a Gaussian curve to a user-determined number of points across a peak and then integrates to determine the area under the curve. Mode 5 determines a single peak intensity at a preset wavelength position.

In selecting an analytical mode, the user must balance improvements in signal reproducibility against increased analysis time. The latter is an important consideration as Ar supplies are limited aboard the *JOIDES Resolution*. Modes 1 and 2 theoretically compensate for instability in the peak position during a run that might result from the constant movement and vibration of the ship. These two modes require significantly greater counting times and consequently use more Ar. Analysis by Mode 5 is quicker by a factor of ~3 but may be more susceptible to signal instability if the peak position is not relocated exactly by the spectrometer throughout the entire run. We adopted Mode 5 for all Leg 187 ICP-AES analyses because of our need to limit Ar consumption. Because of the Ar limitation, we were unable to fully evaluate the other modes.

Plasma Instability

Before Site 1155 (sample run Leg187D), plasma instability led to signal noise and significantly reduced data quality. By increasing the sample dilution factor, filtering sample solutions, and replacing the V groove with the concentric nebulizer, we significantly improved plasma stability. Improper operation of the Ar humidifier may also have contributed to plasma instability and signal noise. Humidified Ar is used to inhibit the precipitation of salts around the capillary orifice within the nebulizer. We observed, however, that condensed water from the humidifier would fill the Ar flow line at the connection to the nebulizer after relatively short periods (<1 hr) of instrument operation. The Ar stream would then bubble through the water into the nebulizer, causing erratic sample aspiration, resulting in random negative spikes in the emission signal.

Following sample run Leg 187D the Ar humidifier was turned off, and there were no further significant negative spikes in the emission signal. With the Ar humidifier off, however, salt buildup around the capillary orifice within the nebulizer gradually decreased the Ar flow

throughout each run (see the "Nebulizer flow" values for sample run Leg187E in Table T6). The salt buildup does not entirely block the capillary orifice, and the flow of sample solution through the nebulizer remains constant. The combined effect of decreasing Ar flow and constant sample flow results in a steady increase in peak and background intensities. As this drift is steady and smooth through the sample run, we accounted for it by applying a linear drift correction (see "Sample Run Format and Data Reduction," p. 17).

Another source of plasma instability specific to the alkali elements Na and K and the JY instrument results from variability in the sheath gas flow. The light emission from these elements originates lower within the plasma; the JY2000 compensates by increasing the Ar gas flow through the torch, which effectively lifts the plasma so that the Na and K emissions are positioned at an optimal viewing height. We found that the sheath Ar gas flow in this instrument is subject to both short- and long-term variations. These variations in Ar gas flow cause short-term noise and long-term drift in Na and K signals. Decreases in the measured intensity for Na and K ranged up to 80% in sample run Leg187E. Several times during Leg 187 the sheath gas flow had to be adjusted. The ideal Ar gas flow of 0.8 L/min was difficult to obtain because the adjustment screw is very sensitive. In general, percent RSD and signal strength improved greatly after the sheath gas flow was adjusted to an ideal rate of 0.8 L/min. The source of both short-and long-term variations of the sheath gas flow is suspected to be related to a faulty Ar gas flow valve.

REFERENCES

Cannat, M., Karson, J.A., Miller, D.J., et al., 1995. *Proc. ODP, Init. Repts.,* 153: College Station, TX (Ocean Drilling Program).

Christie, D.M., West, B.P., Pyle, D.G., and Hanan, B., 1998. Chaotic topography, mantle flow and mantle migration in the Australian-Antarctic Discordance. *Nature,* 394:637–644.

Coffin, M.F., Frey, F.A., Wallace, P.J., et al., 2000. *Proc. ODP, Init. Repts.,* 183 [CD-ROM]. Available from: Ocean Drilling Program, Texas A&M University, College Station, TX 77845-9547, U.S.A.

Dick, H.J.B., Erzinger, J., Stokking, L.B., et al., 1992. *Proc. ODP, Init. Repts.,* 140: College Station (Ocean Drilling Program).

Govindaraju, K., 1989. 1989 compilation of working values and sample description for 272 geostandards. *Geostand. Newsl.,* 13 (spec. iss.).

————, 1994. 1994 compilation of working values and sample description for 383 geostandards. *Geostand. Newsl.,* 18 (spec. iss.).

Klein, E.M., Langmuir, C.H., Zindler, A., Staudigel, H., and Hamelin, B., 1988. Isotope evidence of a mantle convection boundary at the Australian-Antarctic Discordance. *Nature,* 333:623–629.

Larsen, H.C., Saunders, A.D., Clift, P.D., et al., 1994. *Proc. ODP, Init. Repts.,* 152: College Station, TX (Ocean Drilling Program).

Munsell Color Company, Inc., 1975. *Munsell Soil Color Charts:* Baltimore, MD (Munsell).

Norrish, K., and Hutton, J.T., 1969. An accurate X-ray spectrographic method for the analysis of a wide range of geological samples. *Geochim. Cosmochim. Acta,* 33:431–453.

Plumlee, G., 1998a. United States Geological Survey Certificate of Analysis: Basalt, Columbia River, BCR-2 [Online]. Available from World Wide Web: **http://minerals.cr.usgs.gov/geochem/basaltbcr2.html**. [1999–11–08]

————, 1998b. United States Geological Survey Certificate of Analysis: Basalt, Hawaiian Volcanic Observatory, BHVO-2 [Online]. Available from World Wide Weg: **http://minerals.cr.usgs.gov/geochem/basaltbhvo2.html**. [1999–11–08]

Pyle, D.G., 1994. Geochemistry of mid-ocean ridge basalt within and surrounding the Australian Antarctic Discordance [Ph.D. dissert.]. Oregon State Univ., Corvallis.

Pyle, D.G., Christie, D.M., and Mahoney, J.J., 1992. Resolving an isotopic boundary within the Australian-Antarctic Discordance. *Earth Planet. Sci. Lett.,* 112:161–178.

Pyle, D.G., Christie, D.M., Mahoney, J.J., and Duncan, R.A., 1995. Geochemistry and geochronology of ancient southeast Indian and southwest Pacific seafloor. *J. Geophys. Res.,* 100:22261–22282.

Ramsey, M.H., Potts, J.P., Webb, P.C., Watkins, P., Watson, J.S., and Coles, B.J., 1995. An objective assessment of analytical method precision: comparison of ICP-AES and XRF for the analysis of silicate rocks. *Chem. Geol.,* 124:1–19.

Reynolds, R.C., Jr., 1963. Matrix corrections in trace element analysis by X-ray fluorescence: estimation of the mass absorption coefficient by Compton scattering. *Am. Mineral.,* 48:1133–1143.

————, 1967. Estimation of mass absorption coefficients by Compton scattering: improvement and extension of the method. *Am. Mineral.,* 52:1493–1502.

Rock-Color Chart Committee, 1991. *Rock Color Charts.* Geol. Soc. Am.

Sparks, J.W., and Zuleger, E., 1995. *Data report:* Chemical analyses of the Leg 140 reference sample. *In* Erzinger, J., Becker, K., Dick, H.J.B., Stokking, L.B. (Eds.), *Proc. ODP, Sci. Results,* 137/140: College Station, TX (Ocean Drilling Program), 353–355.

Taira, A., Hill, I., Firth, J.V., et al., 1991. *Proc. ODP, Init. Repts.,* 131: College Station, TX (Ocean Drilling Program).

Walker, D., 1973. Behavior of X-ray mass absorption coefficients near absorption edges: Reynold's method revisited. *Am. Mineral.,* 58:1069–1072.

Wessel, P., and Smith, W.H.F., 1995. New version of the Generic Mapping Tools released. *Eos,* 76:329.

Williams, H., Turner, F.J., and Gilbert, C.M., 1982. *Petrography: An Introduction to the Study of Rocks in Thin Sections* (2nd ed.): New York (Freeman).

Figure F1. Diagram illustrating terms used in the discussion of coring operations and core recovery.

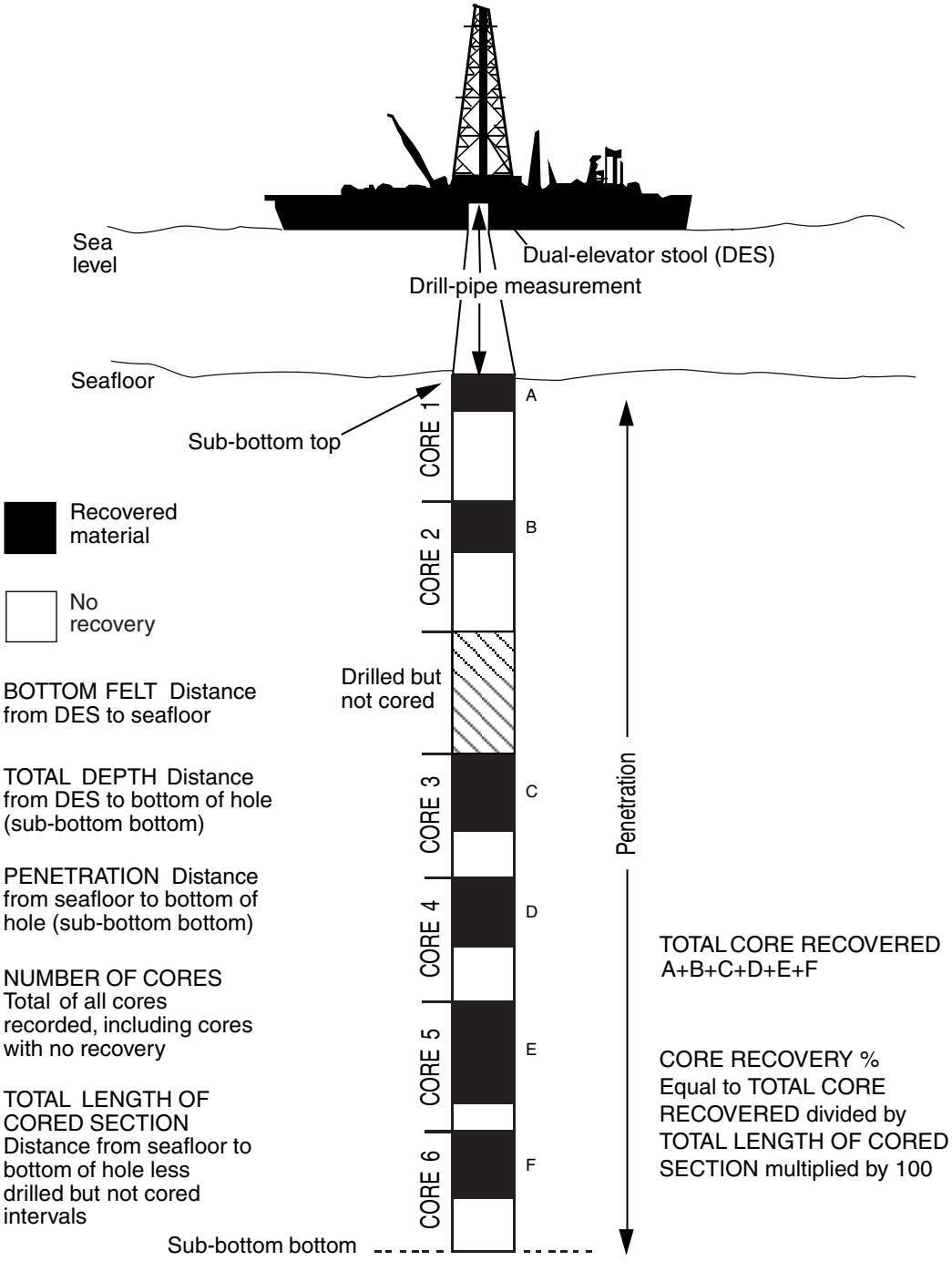

Figure F2. Core curation procedures for hard rocks. Letters designating hole and piece numbers are for illustration only. For example, Leg 187, Site 1155, Hole Q, Pieces A, B, C, D, E, and F would become interval 187-1155Q-1R-1 (Pieces 1–6). Pieces G and H can be reoriented to fit along a fracture, so they are curated as a single piece. In this case, the reassembled single piece is too long to fit in the bottom of Section 1R-1, so it is shunted to the top of Section 1R-2 and curated as interval 187-1155Q-1R-2 (Pieces 1A and 1B). Similarly, Pieces L and M are too long too fit in the bottom of Section 1R-2 after realignment and are shunted to the top of Section 1R-3. Spacers between pieces also artificially add length to the core when measured for archiving and curation. For example, Pieces L and M represent an interval from 2.17 to 2.63 m down from the top of the core as removed from the core barrel but are archived as interval 187-1155Q-1R-3 (Pieces 1A and 1B, 0.0–46.0 cm).

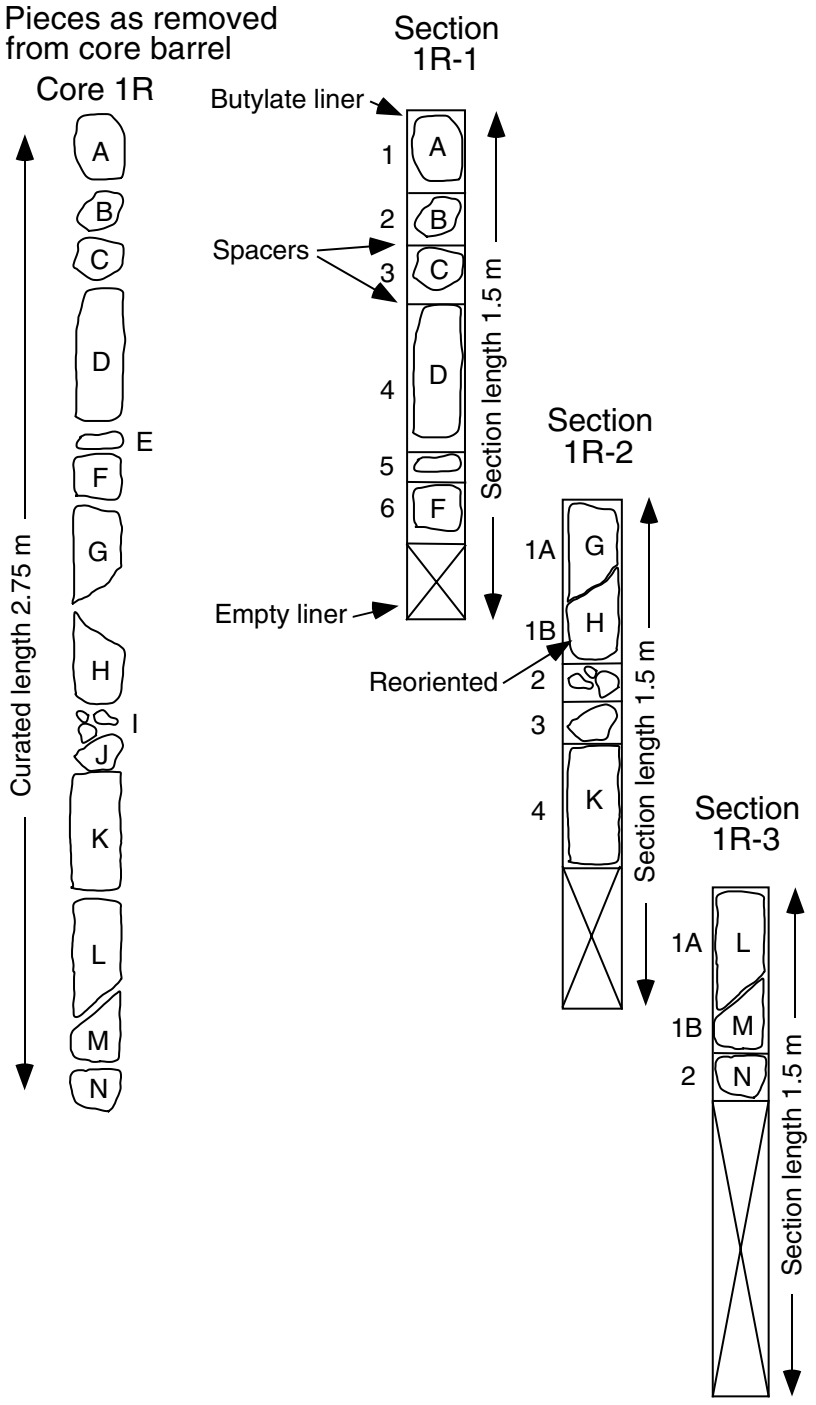

Figure F3. Example of a basalt HRVCD form.

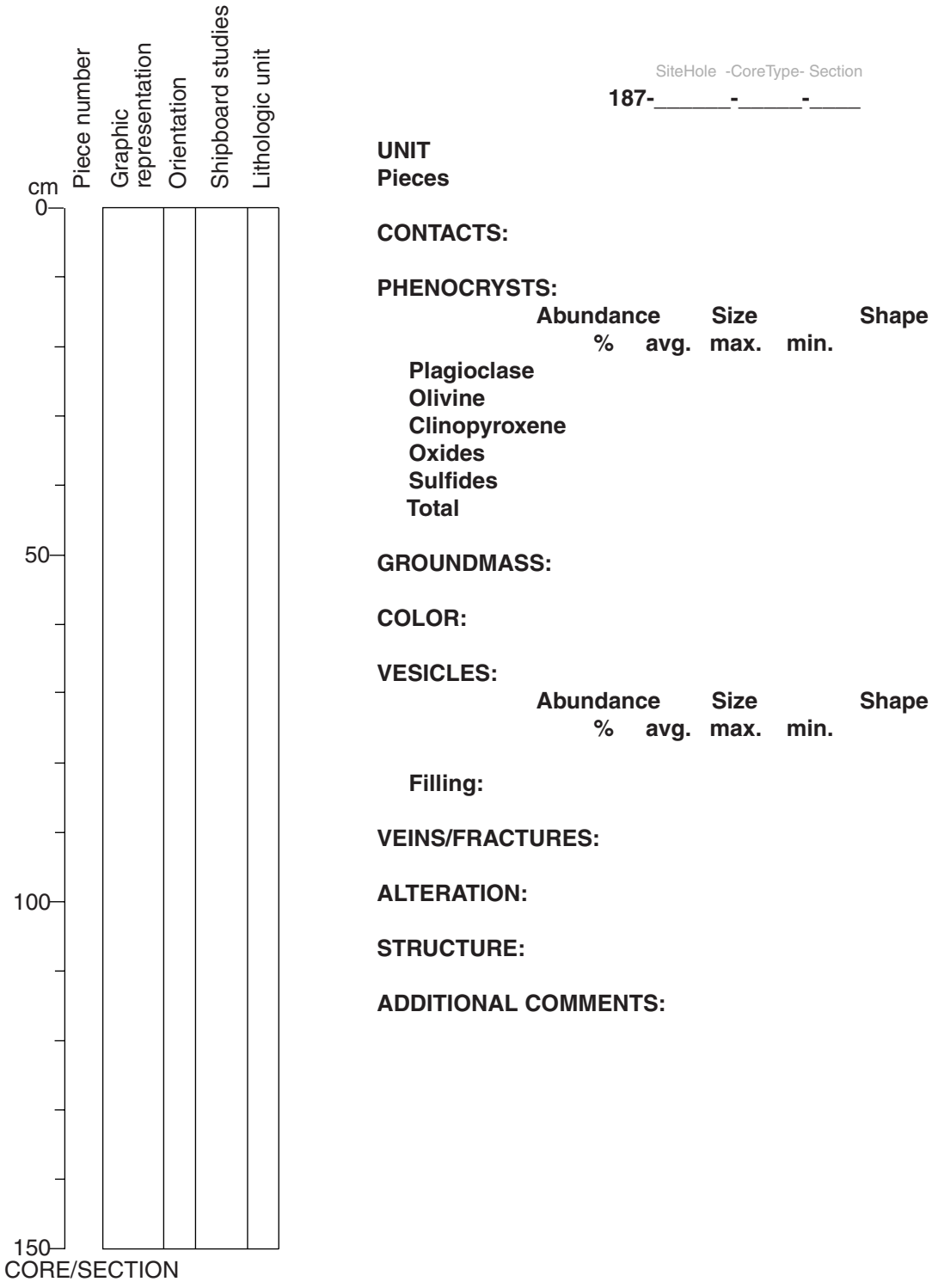

Figure F4. Example of a structural geology description form (see the **"Core Descriptions"** contents list for structural description forms for each site).

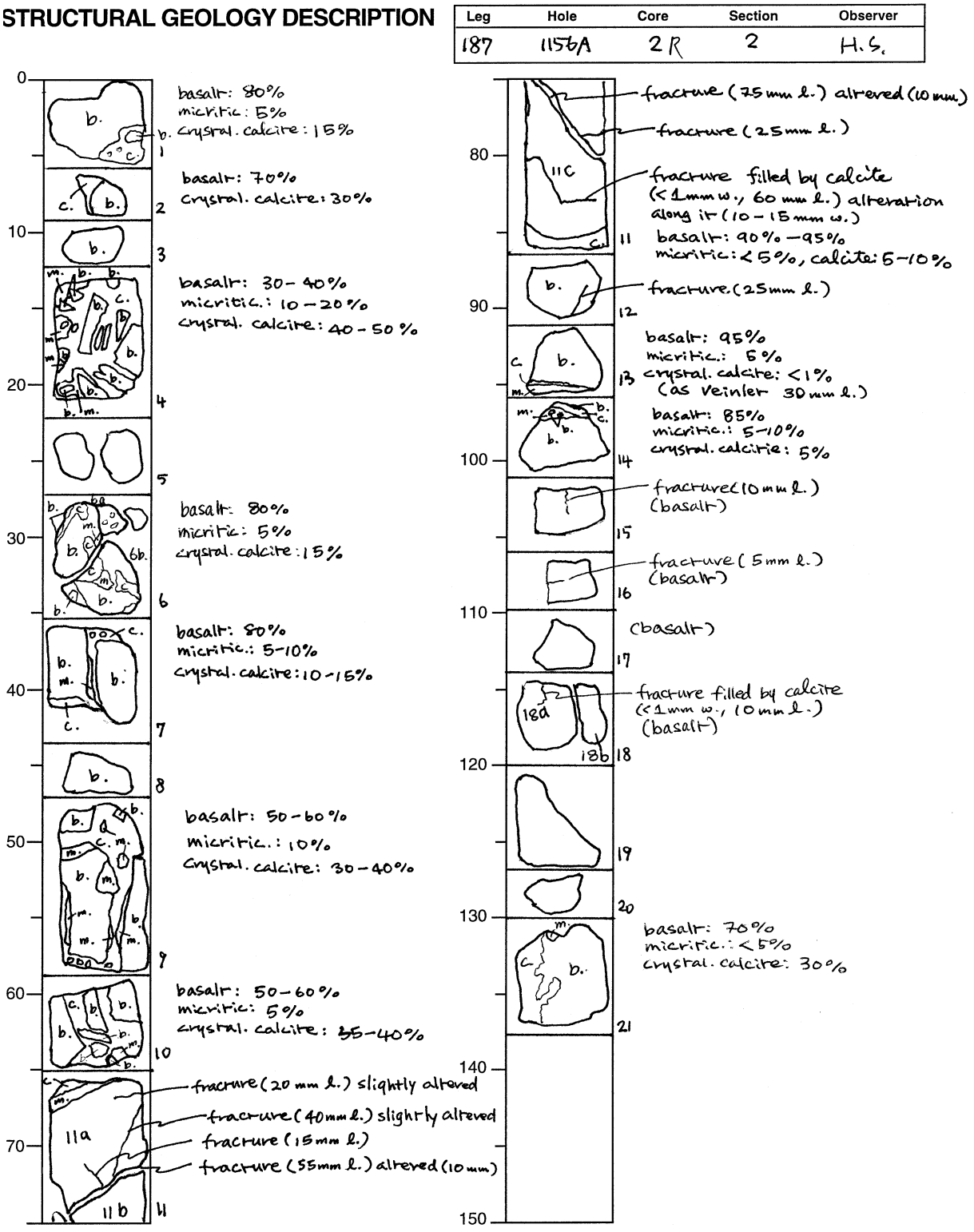

Figure F5. Example of the structural geology log.

STRUCTURAL DATA								DEFORMATION INTENSITY						ORIENTATION													
														PLANES												LINES	
Hole	Core	Section Number	Piece Number	Distance from top to top of the section	Distance from top to the bottom of the section	Distance from top of the section to structure	Depth of the structure	Breccias	Faults (slip: n,r,d,s)	Cataclastic Fabrics	Vein and fracture	Thickness	Length	Orientation on Working Half Face		2nd apparent orientation or strike on horizontal plane		Pole of the plane (core ref. frame)		Strike (core ref. frame)		Strike and dip (geographic ref. frame)		Pitch in the foliation plane	Orientation in the core reference frame	
				(cm)	(cm)	(cm)	(mbsf)	B	F	Cf		mm	mm	dip 1	dir.1	dip 2	dir.2	dir.	dip	strike	dip	strike	dip	pitch	trend	plun.
1152A	1R	1	1	0	76	-	-				0	<1														
			3	0	76	29	0.29				0	<1														
			6	0	76	47	0.47				0	0														
			10	0	76	-	-				0	0														
1152B	2R	1	1	0	58	0	22.50				0	2														
			4	0	58	20	22.70				0	2														
			9	0	58	42	22.92				0	0														
1152B	3R	1	1	4	22	5	27.89				0	<1														
			1	4	22	8	27.92				0	1														
1152B	4R	1	4	0	150	23	36.03				0	0														
			7	0	150	-	-				0	0														
			8	0	150	46	36.26				0	0														
			11	0	150	-	-				0	0														
			19	0	150	118	36.98				0	0														
			23	0	150	140	37.20				0	0														
1152B	4R	2	6	150	184	30	37.60				0	0														
1152B	5R	1	6	0	150	30	41.10				0	0														
			7	0	150	33	41.13				0	0														
			11	0	150	-	-				0	0														
			12	0	150	64	41.44				0	0														
			13	0	150	70	41.50				0	0														
			19	0	150	109	41.89				0	0														
			25	0	150	143	42.23				0	0														
			25	0	150	145	42.25				0	0														
1152B	5R	2	2	150	168	6	42.36				0	0														
			3	150	168	15	42.45				0	0														
1152B	6R	1	2	0	50	-	-				0	0														
			7	0	50	48	45.78				0	0														

Figure F6. Convention used to orient structures.

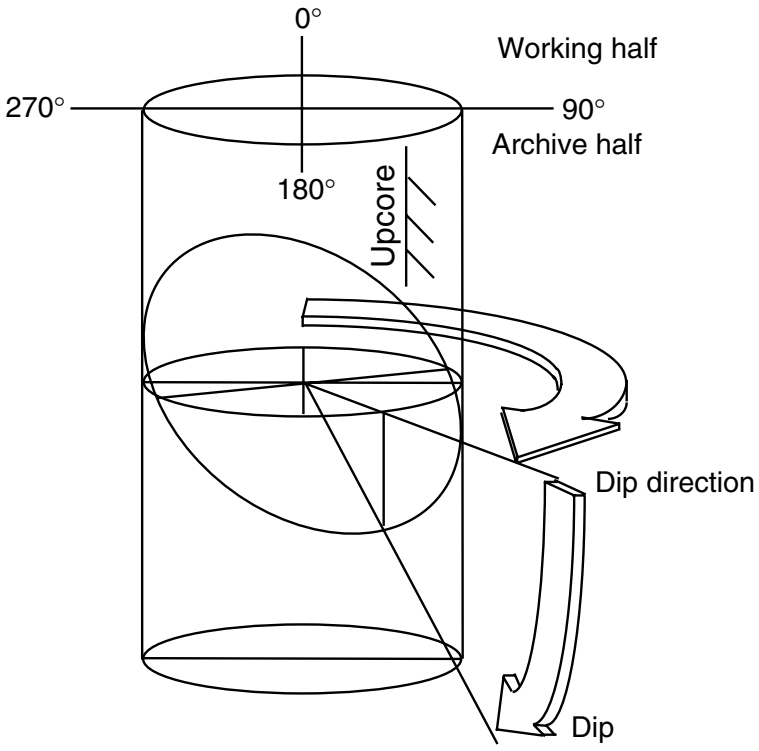

Figure F7. A. Variations in Zr/Ba vs. Ba of basaltic glass dredged from 0- to 7-Ma seafloor within and east of the Australian Antarctic Discordance (AAD) (D.G. Pyle and D.M. Christie, unpubl. data). PRT = propagating rift tip lavas; MORB = mid-ocean-ridge basalts; dashed line separates Indian- and Pacific-type zero-age Southeast Indian Ridge (SEIR) basalt glass. **B.** Variations in Na_2O/TiO_2 vs. MgO of basaltic glass dredged from 0- to 7-Ma seafloor within the AAD and Zone A (D.G. Pyle and D.M. Christie, unpubl. data). Dashed line separates Indian- and Pacific-type zero-age SEIR basalt glass.

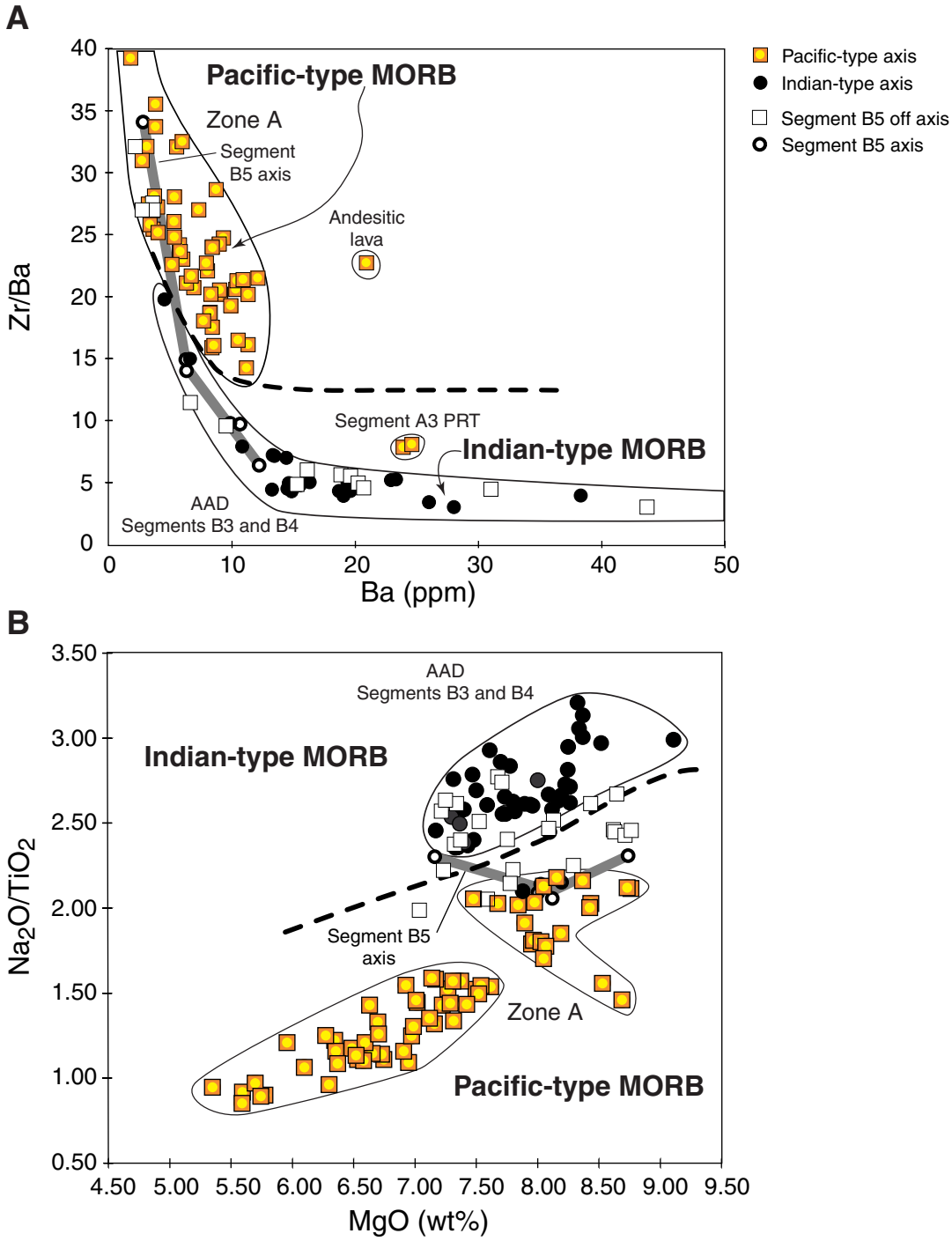

Figure F8. Major element variations in lavas dredged from 0- to 7-Ma seafloor within and east of the Australian Antarctic Discordance (AAD). These data are the baseline for comparison with Leg 187 site results (D.G. Pyle and D.M. Christie, unpubl. data).

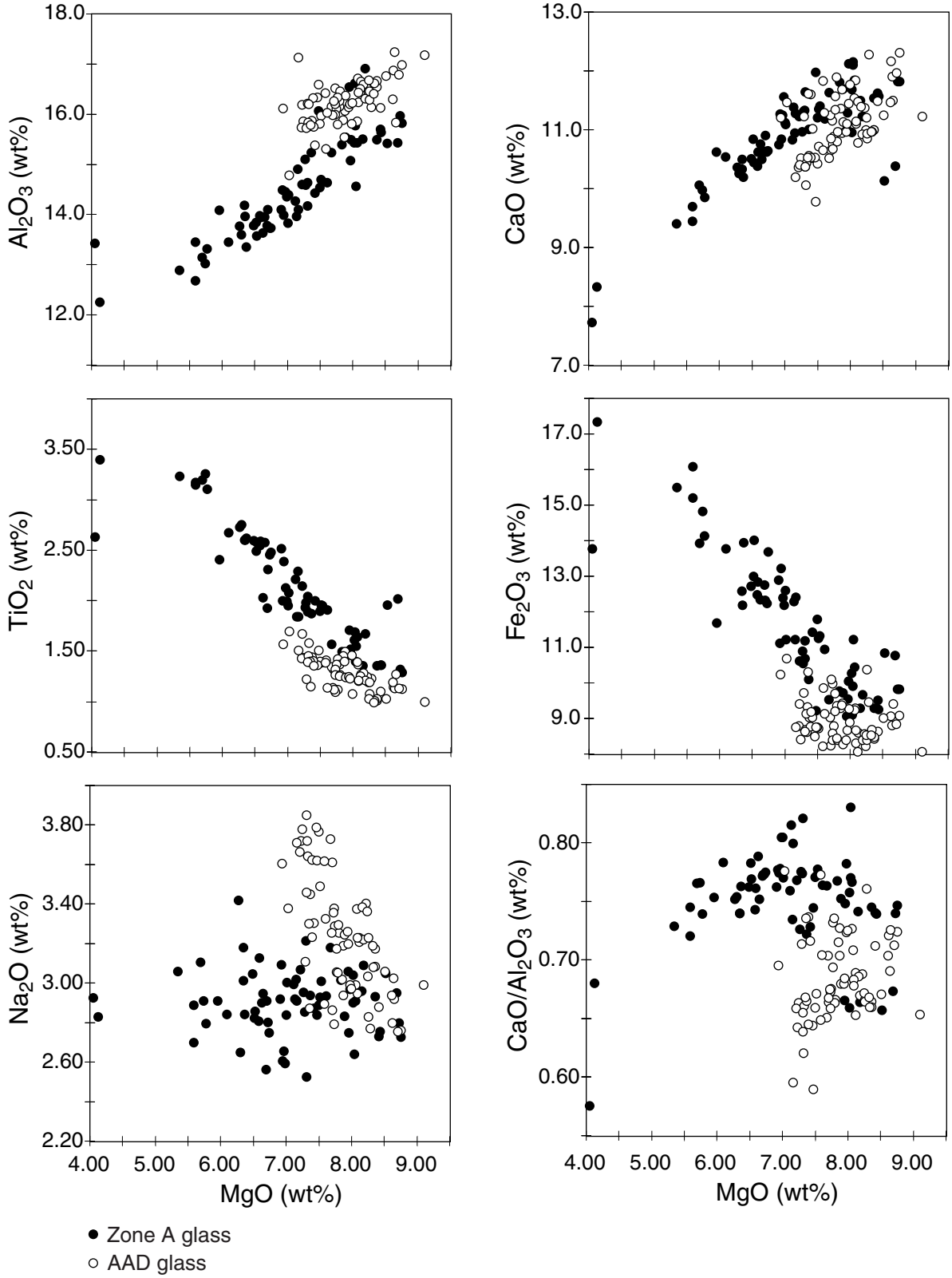

Figure F9. Trace element variations in lavas dredged from 0- to 7-Ma seafloor within the Australian Antarctic Discordance (AAD) and Zone A. These data are the baseline for comparison with Leg 187 site results (D.G. Pyle and D.M. Christie, unpubl. data).

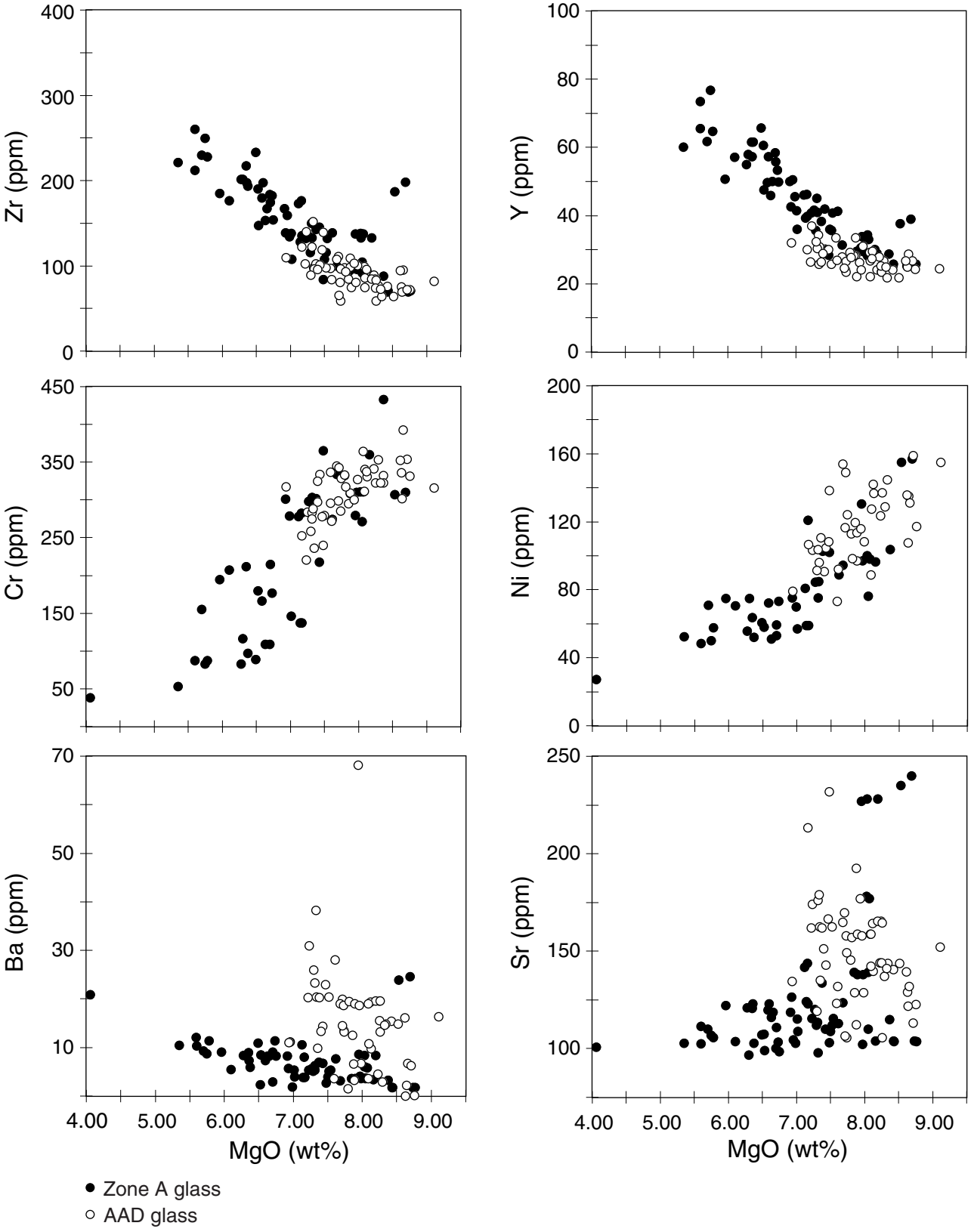

Figure F10. A. Variations in $^{206}Pb/^{204}Pb$ along the Southeast Indian Ridge between 115°E and 140°E. The present position of the isotope boundary between Indian- and Pacific-type mid-ocean-ridge basalt provinces is located at ~126°E. These data are taken from Klein et al. (1988), Pyle et al. (1992), and Pyle et al. (1995). AAD = Australian Antarctic Discordance. **B.** Variations of Zr/Ba vs. $^{206}Pb/^{204}Pb$ showing the data distribution for determining Indian- and Pacific-type mantle provinces. These data are taken from Klein et al. (1988), Pyle et al. (1992), Pyle (1994), Pyle et al. (1995), and D.G. Pyle and D.M. Christie (unpubl. data).

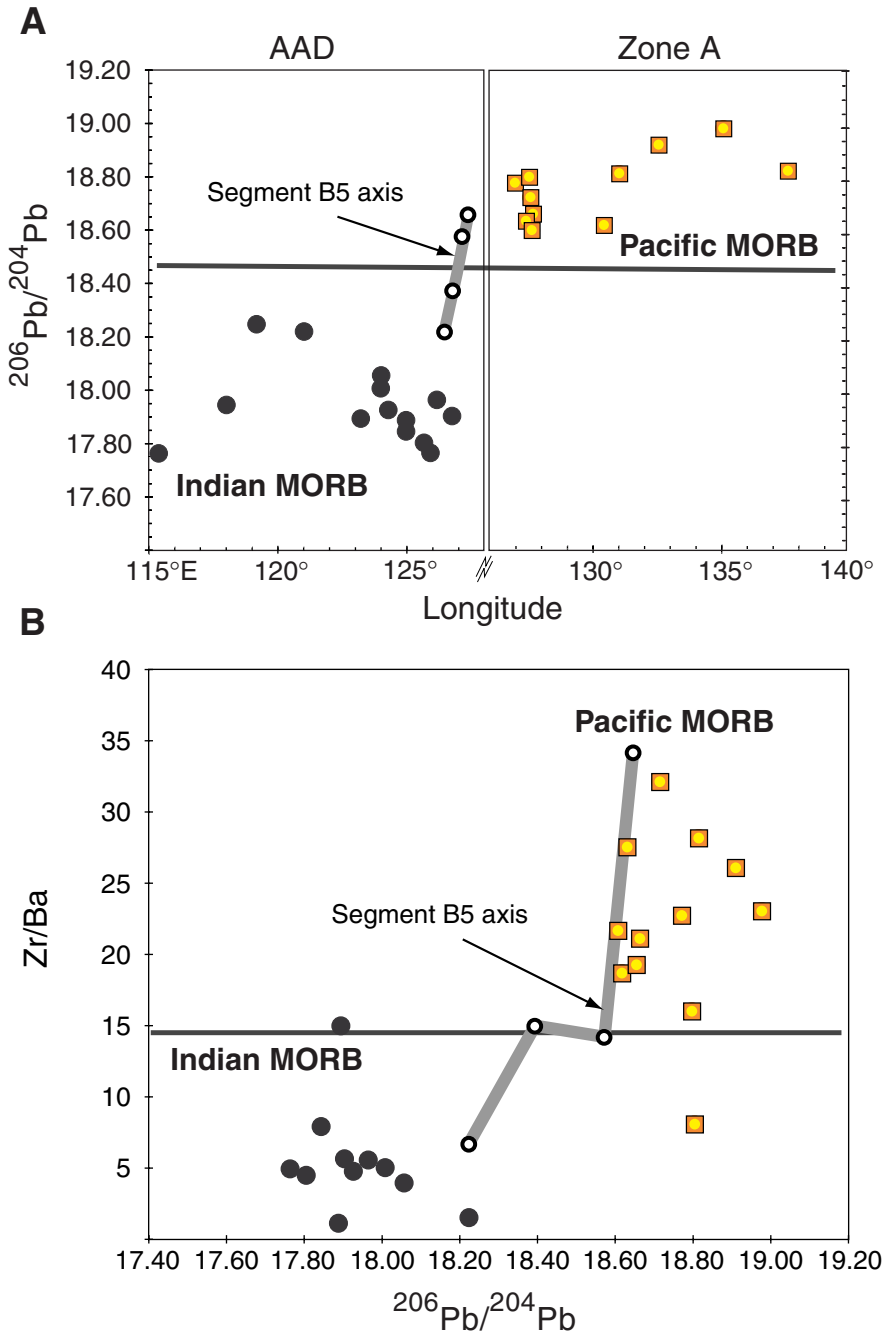

Table T1. Groundmass textural terms, Leg 187.

Textural term	Textural definition
Quench textures	
Glassy	Matrix is amorphous basaltic glass with no visible incipient crystallization.
Spherulitic	Texture is characterized by the presence of spherulites, which are spherical bodies that usually consist of radiating plagioclase and/or clinopyroxene microlites or crystals; individual crystals are indistinguishable with the microscope. These range from discrete spherulites (i.e., individual spherulites separated by glass) to coalesced spherulites (i.e., where spherulites are so abundant they are in contact with one another and the amount of glass is small).
Sheaf	A bundled arrangement of small crystals assuming sheaflike appearance; a central axis of growth often occurs. Sheaf texture ranges from immature (crystals cannot be individually distinguished with the microscope) to mature (discrete skeletal crystals can be distinguished with the microscope). Mineralogically, sheaf textures tend to be dominated by plagioclase.
Plumose	Plume or featherlike arrangement of microlites or crystals; may grade from immature to mature (as in sheaf texture) according to crystal size. Mineralogically, plumose textures tend to be dominated by clinopyroxene.
Groundmass textures	
Intersertal	A term applied to volcanic rocks wherein a base (mesostasis or glass and small crystals) fills the interstices between unoriented feldspar laths, the base forming a relatively small proportion of the rock.
Intergranular	A term applied to volcanic rocks in which there is an aggregation of grains of clinopyroxene, not in parallel optical continuity between a network of feldspar laths, that may be divergent, subradial, or subparallel. Distinguished from an intersertal texture by the absence of interstitial glass or other quenched phases filling the interstices between the feldspar laths.
Subophitic	Said of the ophitic texture of an igneous rock in which the feldspar crystals are approximately the same as the size of the pyroxene and are only partially included by them.
Ophitic	A term applied to textural characteristics in which euhedral or subhedral crystals of plagioclase appear to be entirely enclosed in anhedral to subhedral augite.

Table T2. Structural geology checklist.

- Fractures
  - Fracture density per piece
- Veins
  - Vein orientation
  - Average vein width
  - Mineral infilling
  - Vein fabric
  - Crack seal events (number)
  - Vein density per piece
- Wall rock alteration
  - Width
  - Characteristics of halo
  - Crosscutting relations of veins
    - Vein array
      - Thickness
      - Number of veins
      - Composition of veins
      - Orientation
- Shear zones
  - Orientation
  - Shear zone thickness
  - Lineations
    - Deformation bands
      - Color
      - Thickness
      - Mineral composition
      - Number of bands in array
- Faults
  - Orientation of fault zone
  - Fault zone thickness
  - Shear sense
    - Offset
    - Riedel shears
    - Mineral lineation
  - Amount of offset
  - Nature of gouge
  - Composition of mineral infilling
  - Slickenlines orientation
- Cataclasites
  - Clast
    - Size
    - Shape
    - Composition
  - Matrix composition (gouge or secondary minerals)
- Breccias
  - Matrix or clast supported
  - Percent matrix
  - Matrix composition
  - Clast size
  - Angular vs. rounded clasts
  - Clast composition
  - Origin
    - Hydraulic
    - Fault
- Igneous Contacts
  - Chilled margins
  - Dike width
- Crosscutting relations

Note: This table is also available in **ASCII** format.

Table T3. X-ray fluorescence operating conditions during XRF analyses.

Oxide or element	Line	Crystal	Detector	Collimator	Peak angle (°2θ)	Background offset (°2θ)	Count time	
							Peak (s)	Background (s)
Major element (wt%)								
SiO_2	Kα	PET	FPC	Medium	109.21		40	
TiO_2	Kα	LIF200	FPC	Fine	86.14		40	
Al_2O_3	Kα	PET	FPC	Medium	145.12		100	
Fe_2O_3	Kα	LIF200	FPC	Fine	57.52		40	
MnO	Kα	LIF200	FPC	Fine	62.97		100	
MgO	Kα	TLAP	FPC	Medium	45.17	±0.80	150	150
CaO	Kα	LIF200	FPC	Medium	113.09		40	
Na_2O	Kα	TLAP	FPC	Medium	54.10	–1.20	150	150
K_2O	Kα	LIF200	FPC	Medium	136.69		100	
P_2O_5	Kα	GE111	FPC	Medium	141.04		100	
Trace element (ppm)								
Rh	Kα Compton	LIF200	Scint		18.58		60	
Nb	Kα	LIF200	Scint	Fine	21.40	+0.35	200	100
Zr	Kα	LIF200	Scint	Fine	22.55	–0.35	100	50
Y	Kα	LIF200	Scint	Fine	23.80	–0.40	100	50
Sr	Kα	LIF200	Scint	Fine	25.15	–0.40	100	50
Rb	Kα	LIF200	Scint	Fine	26.62	–0.60	100	50
Zn	Kα	LIF200	Scint	Medium	41.81	–0.55	100	50
Cu	Kα	LIF200	Scint	Fine	45.03	–0.55	100	50
Ni	Kα	LIF200	Scint	Medium	48.67	–0.60	100	50
Cr	Kα	LIF200	FPC	Fine	69.35	–0.50	100	50
V	Kα	LIF220	FPC	Fine	123.06	–0.50	100	50

Notes: All major elements measured using a rhodium X-ray tube operated at 30 kV and 80 mA. Trace elements are measured using a rhodium X-ray tube operated at 60 kV and 50 mA. FPC = flow-proportional counter (P10 gas); Scint = NaI Scintillation counter. This table is also available in **ASCII** format.

Table T4. X-ray fluorescence major element analytical accuracy and precision.

Run	Date (Dec 1999)	Major element (wt%)										Total
		SiO_2	TiO_2	Al_2O_3	Fe_2O_3	MnO	MgO	CaO	Na_2O	K_2O	P_2O_5	
AII-92												
Compilation value*		**50.00**	**1.75**	**15.49**	**10.85**	**0.18**	**7.41**	**11.16**	**3.07**	**0.17**	**0.16**	**100.24**
1	6	49.01	1.71	15.44	10.77	0.17	7.31	10.89	3.14	0.17	0.17	98.78
2	7	49.51	1.77	15.58	10.80	0.18	7.33	10.94	3.13	0.18	0.17	99.59
3	7	49.30	1.79	15.57	10.82	0.18	7.31	10.90	3.11	0.18	0.17	99.33
4	8	49.21	1.69	15.50	10.82	0.17	7.32	10.95	3.15	0.17	0.17	99.15
5	9	49.42	1.75	15.63	10.83	0.17	7.38	10.91	3.15	0.18	0.17	99.59
7	13	49.05	1.74	15.62	10.78	0.17	7.28	10.89	3.14	0.18	0.18	99.03
8	13	49.32	1.77	15.66	10.80	0.18	7.34	10.92	3.15	0.18	0.17	99.49
9	13	49.13	1.75	15.63	10.73	0.17	7.36	10.91	3.17	0.18	0.17	99.20
10	16	49.24	1.84	15.75	10.79	0.19	7.34	10.88	3.06	0.19	0.17	99.45
11	17	49.23	1.75	15.45	10.81	0.18	7.30	10.88	3.24	0.18	0.17	99.19
13	20	48.99	1.76	15.49	10.85	0.17	7.30	10.89	3.15	0.18	0.17	98.95
15	28	50.02	1.68	15.04	10.37	0.16	7.28	10.92	3.40	0.18	0.18	99.23
16	28	50.31	1.74	15.16	10.37	0.17	7.42	10.98	3.40	0.19	0.18	99.92
17	29	50.67	1.72	15.20	10.48	0.17	7.45	11.07	3.38	0.18	0.18	100.50
18	29	50.43	1.72	15.22	10.44	0.17	7.45	11.07	3.44	0.18	0.18	100.30
19	29	50.67	1.74	15.16	10.49	0.17	7.46	11.09	3.43	0.18	0.18	100.57
20	29	50.89	1.73	15.11	10.47	0.17	7.44	11.09	3.40	0.18	0.18	100.66
20	29	50.67	1.68	15.06	10.48	0.17	7.43	11.07	3.39	0.18	0.18	100.31
	Average:	**49.73**	**1.74**	**15.40**	**10.66**	**0.17**	**7.36**	**10.96**	**3.25**	**0.18**	**0.17**	
	1 SD:	0.69	0.04	0.24	0.18	0.01	0.06	0.08	0.14	0.00	0.01	
	%RSD:	1.38	2.27	1.53	1.72	3.87	0.87	0.73	4.18	2.69	2.93	
MRG-1												
Recommended value**		**39.12**	**3.77**	**8.47**	**17.94**	**0.17**	**13.55**	**14.70**	**0.74**	**0.18**	**0.08**	**98.72**
1	6	39.61	3.79	8.79	17.94	0.17	13.63	14.90	0.64	0.20	0.06	99.73
2	7	39.88	3.84	8.82	17.95	0.18	13.62	14.90	0.70	0.20	0.07	100.16
3	7	39.69	3.86	8.81	17.95	0.18	13.64	14.88	0.75	0.20	0.06	100.02
4	8	39.52	3.73	8.66	18.01	0.17	13.60	14.92	0.70	0.19	0.06	99.56
5	9	39.66	3.84	8.83	18.00	0.17	13.62	14.90	0.71	0.20	0.07	100.00
7	13	39.60	3.83	8.78	17.97	0.17	13.63	14.86	0.69	0.20	0.07	99.80
8	13	39.69	3.86	8.85	17.93	0.18	13.70	14.88	0.68	0.20	0.06	100.03
9	13	39.56	3.79	8.78	17.90	0.17	13.63	14.90	0.77	0.20	0.07	99.77
10	18	39.43	3.83	8.73	18.04	0.17	13.61	14.89	0.80	0.20	0.07	99.77
11	18	39.34	3.77	8.63	18.05	0.17	13.57	14.91	0.72	0.19	0.07	99.42
12	19	39.13	3.71	8.45	18.07	0.16	13.56	14.88	0.75	0.18	0.07	98.96
13	20	39.36	3.84	8.74	18.05	0.17	13.63	14.88	0.69	0.20	0.07	99.63
	Average:	**39.54**	**3.81**	**8.74**	**17.99**	**0.17**	**13.62**	**14.89**	**0.72**	**0.20**	**0.07**	
	1 SD:	0.20	0.05	0.11	0.06	0.01	0.04	0.02	0.04	0.01	0.00	
	%RSD:	0.50	1.31	1.29	0.31	3.36	0.26	0.11	6.14	3.31	7.39	

Notes: * = Precision has been estimated from means (in weight percent) and from standard deviations (SD) of replicate analyses of the reference standard MRG-1 and the internal standard AII-92. ** = Govindaraju (1994). RSD = relative standard deviation. This table is also available in **ASCII** format.

Table T5. X-ray fluorescence trace element analytical accuracy and precision.

Run	Date (Dec 1999)	Trace element (ppm)											
		Nb	Zr	Y	Sr	Rb	Zn	Cu	Ni	Cr	V	Ce	Ba
BIR-1													
Recommended value*		**1**	**16**	**16**	**108**	**0**	**71**	**126**	**166**	**382**	**313**	**2**	**7**
2	5	2	19	16	108	0	72	126	162	420	306	2	80
3	6	3	18	17	108	1	73	125	159	427	306	4	79
4	7	4	19	17	108	0	72	124	159	432	315	6	78
5	10	3	19	17	108	0	72	125	160	432	315	5	78
6	11	4	19	17	108	0	71	124	157	429	312	6	77
7	13	3	19	17	108	0	71	124	161	395	313	7	4
8	16	4	19	17	108	0	72	125	157	351	257	7	24
	Average:	**3**	**19**	**17**	**108**	**0**	**72**	**125**	**159**	**412**	**303**	**5**	**60**
	1 SD:	1	0	0	0	0	1	1	2	30	21	2	32
	%RSD:	23	2	2	0	143	1	1	1	7	7	30	53
MRG-1													
Recommended value*		**20**	**108**	**14**	**266**	**9**	**191**	**134**	**193**	**430**	**526**	**26**	**61**
2	5	19	99	14	255	6	189	126	177	525	528	32	47
3	6	21	99	14	254	6	188	126	179	518	510	32	46
4	7	21	100	14	254	7	188	125	178	525	514	33	45
5	10	21	100	14	254	7	186	126	178	525	512	32	46
6	11	22	99	13	254	6	185	126	176	519	489	30	52
7	13	20	98	14	255	7	186	126	180	437	497	32	54
8	16	20	99	14	254	6	185	126	177	444	558	30	60
	Average:	**21**	**99**	**14**	**254**	**6**	**187**	**126**	**178**	**499**	**515**	**32**	**50**
	1 SD:	1	1	1	1	0	1	0	1	40	23	1	6
	%RSD:	4	1	4	0	7	1	0	1	8	4	4	12

Notes: Precision has been estimated from means (in parts per million, except for TiO_2) and from standard deviations (SD) of repeated analyses of the reference standards BIR-1 and MRG-1 following the final calibration. * = Govindaraju (1994). RSD = relative standard deviation. This table is also available in **ASCII** format.

Table T6. JY2000 ICP-AES operating conditions and analytical sample run parameters, Leg 187.

Sample designation	Leg187A	Leg187B	Leg187C	Leg187D	Leg187E	Leg187F	Leg187G	Leg187H	Leg187I	Leg187J	Leg187L
Date (1999):	30 Nov 99	2 Dec 99	3 Dec 99	8 Dec 99	13 Dec 99	14 Dec 99	17 Dec 99	19 Dec 99	26 Dec 99	1 Jan 00	5 Jan 00
Nebulizer type:	V-Groove	V-Groove	V-Groove	V-Groove	Concentric	Concentric	Concentric	Concentric	Concentric	Concentric	Concentric
Sample dilution factor:	505	505	505	505	2005	2005	2005	2005	2005	2005	2005
Pump speed (mL/min):	20 (1)	30 (1.5)	30 (1.5)	30 (1.5)	23 (1.2)	23 (1.2)	23 (1.2)	23 (1.2)	23 (1.2)	23 (1.2)	23 (1.2)
Uptake time (s):	40	40	40	40	40	40	40	40	40	40	40
Rinse time (s):	90	90	90	90	90	90	90	90	90	90	90
Power setting (kv):	1000	1000	1000	1000	1000	1000	1050	1050	1050	1050	1050
Ar humidifier:	Yes	Yes	Yes	Yes	No	No	No	No	No	No	No
Nebulizer pressure (bars):	2.5	2.75	2.94	2.94	3	2.75	3	3	3	3	3
Nebulizer flow (starting-ending) (L/min):	?	?	0.64	0.64	0.83–0.41	0.82	0.84	0.83–0.38	0.75–0.60	?	?
G-3 gas flow (L/min):	1	1	0.8 (reset)	0.8	0.8	0.8 (reset)	0.8	0.8	0.8	0.8	0.8
Method conditions											
Mode:	5	5	5	5	5	5	5	5	5		
Number of replicates:	3	3	3	3	3	3	3	3	3		
Counting time (s):	1	1	1	1,(2-Cr,Ni,Na,K)	1,(2-Cr,Ni,Na,K)	1,(2-Cr,Ni,Na,K)	1,(2-Cr,Ni,Na,K)	1,(2-Cr,Ni,Na,K)	1,(2-Cr,Ni,Na,K)	1,(2-Cr,Ni,Na,K)	1,(2-Cr,Ni,Na,K)

Notes: ? = not recorded. This table is also available in **ASCII** format.

Table T7. Element emission lines used during ICP-AES basalt analyses, Leg 187.

Element	Emission line (nm)
Si	251.611
Ti	308.802
Al*	394.401/396.152
Mn	257.610
Fe	259.940
Ba	455.403
Sr	407.771
Ni	231.604
Cr	267.716
Sc	361.384
Mg	279.553
Ca	393.366
Na	589.592
K	766.490
P	178.229
Zr	343.823
Y	371.030
Ge†	265.118

Notes: * = Al emission line changed from 394.401 to 396.152 after sample run Leg 187C. † = used as an internal drift monitor. This table is also available in **ASCII** format.

Table T8. Major and trace element values used for ICP-AES standard curve calibrations, Leg 187.

Standard:	DNC-1	MAR	K1919	BIR-1	W-2	BHVO-2	BCR-2	BAS140
Reference:	1	2	2	1	1	3	3	4
Major element (wt%)								
SiO_2	47.04	49.59	50.00	47.77	52.44	49.90	54.10	50.50
TiO_2	0.48	1.23	2.70	0.96	1.06	2.73	2.26	0.98
Al_2O_3	18.30	15.24	13.85	15.35	15.35	13.50	13.50	14.60
Fe_2O_3	9.93	11.11	12.28	11.26	10.74	12.30	13.80	11.10
MnO	0.15	0.18	0.17	0.17	0.16	0.17	0.20	0.19
MgO	10.05	9.09	7.01	9.68	6.37	7.23	3.59	8.15
CaO	11.27	11.36	11.36	13.24	10.87	11.4	7.12	12.4
Na_2O	1.87	2.56	2.36	1.75	2.14	2.22	3.16	1.84
K_2O	0.23	0.09	0.54	0.03	0.63	0.52	1.79	0.01
P_2O_5	0.09	0.11	0.28	0.05	0.13	0.27	0.35	0.08
H_2O^+	0.68			0.10	0.55			
H_2O^-	0.33			0.07	0.23			
CO2	0.05			0.02	0.06			
Total	100.41	100.56	100.55	100.42	100.67	100.24	99.87	99.85
Trace element (ppm)								
Ba	114	6.55	135	7.7	182	130	683	0.8
Sr	145	91.9	403	108	194	389	346	60.6
Ni	247	150.9	98	166	70	119		128
Cr	285	321	245	382	93	280	18	374
Sc	31	39.3	30.3	44	35	32	33	
Y	18	31.7	26.9	16	24	26	37	19.8
Zr	41	79.1	186	22	94	172	188	40.3

Notes: Standards: MAR = mid-Atlantic Ridge, a Lamont-Doherty Earth Observatory (LDEO) laboratory standard of normal mid-ocean-ridge basalt; K1919 = an LDEO standard equivalent to BHVO-1 generally used as a drift-correcting standard; BAS140 = an ODP internal standard equivalent of a Leg 140, Hole 504B, diabase (Dick, Erzinger, Stokking, et al., 1992; Sparks and Zuleger, 1995). References: 1 = Govindaraju (1994); 2 = LDEO; 3 = Plumlee (1998a, 1998b) - preliminary values; 4 = ODP (1999 shipboard compilation). This table is also available in **ASCII** format.

Table T9. Estimates of accuracy and precision for JY2000 ICP-AES major element analyses.

Sample run or replicate	Date (Dec 1999)	Major element (wt%)										Total
		SiO_2	TiO_2	Al_2O_3	Fe_2O_3	MnO	MgO	CaO	Na_2O	K_2O	P_2O_5	
MW8801-17-26 (whole rock)*												
Probe		50.62	1.36	15.49	9.29	0.15	8.37	11.54	2.93	0.03	0.15	99.93
DCP		50.17	1.29	15.61	9.49	0.16	8.61	11.73	2.83	0.03	0.12	100.04
Leg187A	1	51.27†	1.32	15.21	9.38	0.16	8.56	11.40	2.54	0.04	0.13	100†
Leg187C	3	50.69	1.32	15.21	9.38	0.16	8.56	11.40	2.54	0.04	0.13	99.41
Leg187D.a	8	50.56	1.24	14.80	9.46	0.16	8.45	11.52	2.54	0.03	0.12	98.88
Leg187D.b	8	50.73	1.23	15.16	9.34	0.16	8.20	11.89	2.68	0.05	0.13	99.58
Leg187E.a	13	50.84	1.35	15.38	9.63	0.16	8.59	11.62	2.83	0.04	0.13	100.56
Leg187E.b	13	50.65	1.33	15.59	9.51	0.16	8.46	11.77	2.74	0.04	0.13	100.36
Leg187E.c	13	51.23	1.33	15.76	9.54	0.16	8.46	11.74	2.77	0.04	0.13	101.16
Leg187E.d	13	51.07	1.35	15.75	9.74	0.16	8.61	11.92	2.91	0.03	0.13	101.67
Leg187F.a	14	49.91	1.31	15.25	9.49	0.16	8.54	11.54	2.67	0.04	0.13	99.04
Leg187F.b	14	49.48	1.29	15.42	9.32	0.16	8.45	11.60	2.65	0.04	0.12	98.53
Leg187G.a	17	50.86	1.33	15.33	9.66	0.16	8.45	11.56	2.76	0.05	0.12	100.29
Leg187G.b	17	50.85	1.32	15.35	9.67	0.17	8.67	11.64	3.06	0.04	0.13	100.89
Leg187H.a	20	49.94	1.31	15.57	9.48	0.16	8.31	11.60	2.91	0.05	0.12	99.44
Leg187H.b	20	51.32	1.36	15.64	9.75	0.16	8.58	11.90	2.95	0.05	0.12	101.83
Leg187H.c	20	50.53	1.29	15.40	9.64	0.16	8.55	11.61	2.95	0.05	0.13	100.31
Leg187I.a	26	50.22	1.34	15.47	9.44	0.15	8.42	11.63	2.87	0.06	0.11	99.72
Leg187I.b	26	50.24	1.28	15.24	9.26	0.17	8.26	11.56	3.14	0.06	0.15	99.36
	Average:	**50.61**	**1.31**	**15.38**	**9.51**	**0.16**	**8.48**	**11.64**	**2.79**	**0.05**	**0.13**	
	1 SD:	0.52	0.04	0.24	0.150	0.00	0.13	0.16	0.181	0.009	0.007	
	%RSD:	1.02	2.73	1.57	1.58	2.67	1.49	1.34	6.49	19.62	5.79	
BHVO-2												
Published value		**49.9**	**2.73**	**13.5**	**12.3**	**0.166**	**7.23**	**11.4**	**2.22**	**0.52**	**0.27**	**100.236**
±		0.6	0.04	0.2	0.2		0.12	0.2	0.08	0.01	0.02	
Leg187C	3	48.28†	2.77	14.71	12.33	0.17	7.46	10.99	2.40	0.58	0.31	100†
Leg187D	8	50.08	2.57	12.91	11.98	0.17	7.11	11.27	2.19	0.49	0.28	99.04
Leg187E.a	13	49.50	2.72	14.12	12.10	0.17	7.25	11.50	2.12	0.44	0.28	100.20
Leg187E.b	13	48.92	2.69	14.22	12.18	0.16	7.14	11.41	2.02	0.44	0.28	99.48
Leg187E.c	13	49.86	2.79	14.34	12.32	0.17	7.18	11.52	2.27	0.41	0.28	101.15
Leg187E.d	13	49.40	2.75	14.14	12.51	0.17	7.25	11.52	2.17	0.44	0.27	100.62
Leg187F.a	14	48.97	2.66	13.72	12.07	0.17	7.25	11.26	2.06	0.41	0.27	98.83
Leg187F.b	14	50.05	2.73	13.82	12.31	0.17	7.13	11.46	2.06	0.40	0.24	100.37
Leg187G.a	17	48.93	2.70	13.42	12.32	0.17	7.20	11.23	2.14	0.52	0.27	98.90
Leg187G.b	17	48.63	2.66	13.41	12.10	0.17	7.20	11.12	2.45	0.53	0.31	98.59
Leg187H.a	20	48.83	2.66	13.81	11.98	0.16	7.04	11.27	2.19	0.54	0.25	98.74
Leg187H.b	20	49.62	2.73	13.86	12.04	0.17	7.36	11.53	2.27	0.54	0.28	100.39
Leg187H.c	20	48.21	2.61	13.40	11.81	0.16	7.08	11.08	2.00	0.57	0.29	97.19
Leg187I.a	26	49.06	2.66	13.66	12.10	0.17	7.19	11.21	2.24	0.52	0.26	99.08
	Average:	**49.17**	**2.69**	**13.82**	**12.15**	**0.17**	**7.20**	**11.31**	**2.18**	**0.49**	**0.28**	
	1 SD:	0.61	0.06	0.46	0.185	0.00	0.11	0.18	0.13	0.06	0.018	
	%RSD:	1.23	2.30	3.35	1.52	1.76	1.52	1.59	6.14	13.12	6.40	

Notes: These estimates are derived from replicate analyses of the USGS reference standard BHVO-2 and Zone A SEIR whole-rock basalt sample MW8801-17-26, Leg 187. * = D. Pyle and D. Christie (unpubl. data), microprobe and direct current plasma (DCP) analyses. † = SiO_2 estimated by subtracting the total of the other major elements from 100%. SD = standard deviation, RSD = relative standard deviation. This table is also available in **ASCII** format.

Table T10. Estimates of accuracy and precision for JY2000 ICP-AES trace element analyses.

Sample run or replicate	Date (Dec 1999)	Trace element (ppm) Zr	Y	Sr	Ni	Cr	Ba	Sc
MW8801-17-26 (whole rock)*		88.1	28.7	115	104	433	3.2	37.1
Leg187A	1	88.9	29.8	103.3	90.1	389.7	2.4	
Leg187C	3	88.9	29.8	103.3	90.1	389.7	2.4	
Leg187D.a	8	86.4	30.2	99.3	85.5	381.5	3.4	37.0
Leg187D.b	8	87.4	30.0	103.9	83.4	405.8	3.4	37.0
Leg187E.a	13	84.8	29.7	102.5	99.6	371.9	2.8	36.4
Leg187E.b	13	83.9	30.1	103.3	99.0	357.9	3.0	36.9
Leg187E.c	13	84.0	30.1	103.5	100.7	366.1	3.0	36.6
Leg187E.d	13	85.6	30.2	106.8	97.7	392.2	2.7	37.4
Leg187F.a	14	84.3	30.0	102.4	97.5	391.2	3.5	35.3
Leg187F.b	14	82.3	30.1	101.0	95.2	375.8	3.7	35.9
Leg187G.a	17	85.2	29.5	101.3	94.3	363.0	3.6	37.3
Leg187G.b	17	84.5	31.1	101.5	92.0	355.3	3.4	38.9
Leg187H.a	20	90.8	29.7	104.5	99.3	381.1	3.9	36.9
Leg187H.b	20	90.6	30.8	106.3	95.5	349.1	3.8	38.4
Leg187H.c	20	81.8	29.0	103.9	102.9	383.1	3.8	33.6
Leg187I.a	26	82.8	31.3	107.4	87.7	342.8	2.9	36.1
Leg187I.b	26	89.0	30.1	103.4	94.3	364.8	2.9	37.3
	Average:	**86.0**	**30.1**	**103.4**	**94.4**	**374.2**	**3.2**	**36.7**
	1 SD:	2.9	0.6	2.1	5.6	17.3	0.5	1.3
	%RSD:	3.3	1.9	2.0	5.9	4.6	15.2	3.4
BHVO-2								
Published value		**179**	**27.6**	**389**	**121**	**289**	**130**	**32**
±		11	2	23	7	19	13	1
Leg187C	3	172.6	26.9	391.0	109.2	276.2	138.3	
Leg187D	8	175.8	26.4	395.1	102.3	281.9	132.1	30.3
Leg187E.a	13	170.3	26.8	407.6	111.0	282.7	141.5	30.6
Leg187E.b	13	173.8	26.7	406.8	115.7	283.2	141.4	30.8
Leg187E.c	13	170.4	26.9	406.1	117.5	290.1	144.9	30.9
Leg187E.d	13	171.3	26.4	412.6	115.1	305.9	143.4	30.8
Leg187F.a	14	170.5	26.4	397.6	116.6	298.8	139.3	30.1
Leg187F.b	14	169.5	27.2	401.8	120.3	280.5	142.3	30.8
Leg187G.a	17	173.5	26.1	394.2	118.7	277.5	135.8	32.1
Leg187G.b	17	187.8	29.3	400.0	125.4	287.7	137.6	31.5
Leg187H.a	20	176.6	26.1	403.1	107.6	279.7	140.9	31.5
Leg187H.b	20	178.5	26.0	409.3	132.9	286.1	141.5	32.5
Leg187H.c	20	141.0	23.1	376.6	123.9	305.8	131.4	25.4
Leg187I.a	26	170.6	27.3	414.1	110.8	272.5	141.7	31.8
	Average:	**171.6**	**26.5**	**401.1**	**116.2**	**286.3**	**139.4**	**30.7**
	1 SD:	10.0	1.3	9.9	8.0	10.5	4.0	1.8
	%RSD:	5.9	4.8	2.5	6.9	3.7	2.9	5.7

Notes: These estimates are derived from replicate analyses of the USGS reference standard BHVO-2 and Zone A SEIR whole-rock basalt sample MW8801-17-26, Leg 187. * = D. Pyle and D. Christie (unpubl. data). SD = standard deviation; RSD = relative standard deviation. This table is also available in **ASCII** format.